Changes in Extreme Daily Precipitation over the Contiguous United States from Convection-Permitting Simulations

Sylvia N. Stinnett,[a] Vittorio A. Gensini,[a] Alex M. Haberlie,[a] Allison C. Michaelis,[a] and Walker S. Ashley[a]

[a] *Department of Earth, Atmosphere, and Environment, Northern Illinois University, DeKalb, Illinois*

Corresponding author: Vittorio Gensini, vgensini@niu.edu

File generated with AMS Word template 2.0

Early Online Release: This preliminary version has been accepted for publication in *Journal of Applied Meteorology and Climatology*, may be fully cited, and has been assigned DOI 10.1175/JAMC-D-23-0206.1. The final typeset copyedited article will replace the EOR at the above DOI when it is published.

ABSTRACT

The potential for changes in extreme precipitation events due to anthropogenic climate change may have significant societal impacts (e.g., agricultural productivity, property loss, mortality). This project uses a dynamically downscaled, convection-permitting regional climate model to investigate extreme daily precipitation in the CONUS, defined explicitly as the 99th percentile 24-h accumulated value. The simulation output includes a historical baseline (HIST; 1990–2005) and two epochs at the end of the twenty-first century (EOC; 2085–2100) under intermediate and pessimistic emissions scenarios. Independent observations illustrate that HIST admirably represents extreme precipitation climatology for most locations in the domain. Comparisons between HIST and the two EOC scenarios for the 99th percentile of daily precipitation show statistically significant increases during Dec–May across the Midwest and Ohio Valley and statistically significant decreases for the southern Great Plains during Dec–Feb. Extreme value analysis further reveals increasing variability in precipitation extremes for eight climatologically unique cities across the CONUS by the end of the twenty-first century and significant increases in return period precipitation amounts for most cities examined. These results provide additional guidance for stakeholders to reduce societal impacts and economic loss from daily precipitation extremes and create a more climate-resilient society.

SIGNIFICANCE STATEMENT

This study uses a novel convection-allowing regional climate model to illustrate potential future changes in daily extreme rainfall amounts due to climate change. Future scenarios project robust increases in these events during some seasons for portions of the Midwest and Ohio Valley, whereas the southern Great Plains are projected to experience decreases. Furthermore, we find a notable increase in the variability of extreme daily precipitation across various CONUS cities by the end of the twenty-first century. Overall, our results further our understanding of how extreme precipitation events may change in the future and, therefore, help policy makers and stakeholders adapt to these impactful events.

1. Introduction

The impacts of anthropogenic climate change will be felt most strongly through changes in the intensity and frequency of hazards such as extreme precipitation and resulting floods. Floods are the second deadliest weather-related hazard in the United States, falling just

Accepted for publication in *Journal of Applied Meteorology and Climatology*. DOI 10.1175/JAMC-D-23-0206.1.

behind heat, causing an average of 80–100 flood deaths per year (Ashley and Ashley 2008a, b; Villarini and Slater 2017; Zhou et al. 2018; Lim and Skidmore 2019; Han and Sharif 2021). The United States recorded 40 separate flood disasters from 1980–2022 (excluding inland flood damage caused by tropical cyclones), each resulting in at least $1 billion in consumer price index (CPI) adjusted losses (NCEI 2023). Those billion-dollar flood disasters, on average, produced $4.3 billion in monetary loss (CPI-adjusted) and are comparable to other studies showing average annual losses in the $4–9 billion range (Villarini and Slater 2017; Zhou et al. 2018; National Academies of Sciences, Engineering, and Medicine 2019; NCEI 2023). As of 2011, the observed increase in economic losses had not been directly related to anthropogenic climate change, but rather largely attributed to socioeconomic factors such as increasing exposure and the "expanding bull's-eye effect" (Bouwer 2011; Ashley et al. 2014; Strader and Ashley 2015). Therefore, there is still an increasing risk of flooding and losses with increasing vulnerability due to projected land use and exposure changes (Strader and Ashley 2015; Ferguson and Ashley 2017; Andreadis et al. 2022; Rashid et al. 2023).

Overall and extreme precipitation has been increasing globally over the past several decades (e.g., Dai et al. 2004; Groisman et al. 2005; Alexander et al. 2006; Min et al. 2011; O'Gorman 2012; Westra et al. 2013; Papalexiou and Montanari 2019). More than 50% of global stations showed increasing precipitation trends, and the midlatitudes, in particular, have experienced an increased frequency of extreme precipitation events and a tendency for wetter conditions (Groisman et al. 2005; Alexander et al. 2006; Min et al. 2011; Westra et al. 2013; Papalexiou and Montanari 2019). In the CONUS, there has been a statistically significant upward trend in precipitation over the last ~100 years, especially in the Midwest, Southeast, and Northeast (e.g., Groisman et al. 2005; Alexander et al. 2006; Groisman et al. 2012; Kunkel et al. 2013a; Janssen et al. 2014; Huang et al. 2017; Changnon and Gensini 2019; Fowler et al. 2021). For many regions, droughts have become shorter in duration, less frequent, and less spatially expansive, except in the Southwest and interior West; however, drying could expand into the low- and mid-latitudes as higher greenhouse gas concentrations increase temperatures and alter sensible and latent heat fluxes (Trenberth et al. 2003; Dai et al. 2004; Mishra and Singh 2010; Dai 2011; Trenberth 2011; Trenberth et al. 2014; Zhang et al. 2021). These studies show a tendency for more extreme conditions in many regions of the CONUS, yet the historical changes are relatively small in comparison to late-twenty-first-century projections.

Accepted for publication in *Journal of Applied Meteorology and Climatology*. DOI 10.1175/JAMC-D-23-0206.1.

The atmospheric response of extreme precipitation to anthropogenic climate change has been researched extensively (e.g., Meehl et al. 2005; Kharin et al. 2007; Allan and Soden 2008; O'Gorman and Schneider 2009; Sugiyama et al. 2010; Pan et al. 2011; Dominquez et al. 2012; Zhu et al. 2013; Janssen et al. 2014; Prein et al. 2017; Huang and Stevenson 2021; Picard et al. 2023). By using emission scenarios—such as representative concentration pathways (RCPs)—one can apply a storyline approach and extensively examine future projections of the atmospheric state and, thus, create climatologies for future scenarios (e.g., Kharin et al. 2007; Kunkel et al. 2013b; Janssen et al. 2014; Hazeleger et al. 2015; Prein et al. 2017; Shepard et al. 2018; Li et al. 2022; Quintero et al. 2022; Gensini et al. 2023; Rashid et al. 2023). For example, North America could experience an increase in mesoscale convective system (MCS) frequency and a 15–40% increase in maximum precipitation rates due to a deeper layer permitting more collision and coalescence (Pan et al. 2011; Trenberth 2011; Prein et al. 2017; Haberlie et al. 2023). Spatiotemporal changes in MCSs can have significant socioeconomic impacts since a large proportion of annual precipitation accumulation stems from these events (e.g., Ashley et al. 2003; Schumacher and Johnson 2006; Stevenson and Schumacher 2014; Feng et al. 2016; Prein et al. 2017; Haberlie and Ashley 2019). Highlighting the potential changes in future extreme precipitation can inform stakeholders so that they may develop effective mitigation and adaptation strategies to reduce impacts.

Adequate horizontal grid spacing of a regional climate model (RCM) is necessary to interpret projected changes in mesoscale processes, such as convective precipitation not well resolved by the relatively coarse horizontal grid spacing of general circulation models (GCM). The process of dynamical downscaling (e.g., Prein et al. 2015) is often employed where a RCM is forced by GCM output to both implicitly and explicitly examine hazardous convective weather, such as extreme precipitation, at a convection-allowing scale (e.g., Trapp et al. 2011; Robinson et al. 2013; Gensini and Mote 2014; Tippet et al. 2015; Hoogewind et al. 2017; Trapp et al. 2019; Haberlie et al. 2022; Ashley et al. 2023; Gensini et al. 2023). RCM simulations at this scale typically show only a single outcome, which makes reaching definitive conclusions challenging unless other experiments (i.e., an ensemble approach) are generated to better discern uncertainty (Gensini et al. 2023). An ensemble approach, however, is challenging to execute due to computational limitations and considerable time expenditure for high-resolution RCM simulations, a limitation that has, until recently, permitted only a few simulations of substantial duration at convection-allowing scales.

Accepted for publication in *Journal of Applied Meteorology and Climatology*. DOI 10.1175/JAMC-D-23-0206.1.

Here, we use a novel dynamically downscaled convection-permitting simulations to examine projected changes in extreme daily precipitation throughout the CONUS during the twenty-first century. The model used herein allows for representation of regional climate change of precipitation extremes closer to the local scales at which they occur (e.g., < 4 km horizontal grid spacing), which is of great interest to stakeholders. Section 2 describes the datasets and methodology used in this study. Results are presented in section 3, with a spatiotemporal analysis of extreme daily precipitation followed by an extreme value analysis (EVA). Finally, a discussion and concluding remarks follow in section 4.

2. Data and methodology

a. RCM output

Our RCM simulations were conducted with the Weather Research and Forecasting Model (WRF-ARW version 4.1.2; Skamarock et al. 2019) configured with a horizontal grid spacing of 3.75 km and 51 vertical levels across the CONUS. WRF-ARW is a fully compressible nonhydrostatic model widely used in both operational forecasting and research (Skamarock and Klemp 2008; Powers et al. 2017). Small horizontal grid spacing (i.e., ≤ 4 km) permits the removal of a convective parameterization scheme, allowing the explicit development of all modes of deep, moist convection (Weisman et al. 1997; Skamarock and Klemp 2008; Westra et al. 2014). Initial and lateral boundary conditions input into the RCM stemmed from the Community Earth System Model (CESM; Hurrell et al. 2013) GCM output, a participant in phase 5 of the Coupled Model Intercomparison Project (CMIP5; Taylor et al. 2012). We used a version of these data from Bruyère et al. (2014) that performed an additional regrid and bias-correction using 1981–2005 ERA-Interim reanalysis (Dee et al. 2011). Spectral nudging was used at 6-h intervals to large-scale (3x; 2y) features for T (temperature), q (specific humidity), u (zonal wind speed), v (meridional wind speed), and Φ (geopotential) above the planetary boundary layer. The complete RCM design and configuration is detailed in Gensini et al. (2023).

RCM simulations were continuously integrated over a hydrologic year (1 October–30 September), with reinitialization each October 1. Simulated time periods include three 15-year epochs, with a historical baseline (HIST; 1990–2005) and two future epochs (EOC; 2085–2100) using RCP4.5 (EOC4.5) and RCP8.5 (EOC8.5) future climate scenarios (Moss et

Accepted for publication in *Journal of Applied Meteorology and Climatology*. DOI 10.1175/JAMC-D-23-0206.1.

al. 2010). These RCPs—used in the Intergovernmental Panel on Climate Change (IPCC) fifth assessment report (AR5; IPCC 2014)—permit the investigation of the atmospheric reaction to different plausible future climates with differing levels of radiative forcings from changes in greenhouse gasses (Moss et al. 2010). RCP4.5 represents a moderate future climate scenario with stabilization of radiative forcing and greenhouse gas concentrations without overshoot by 2100, while RCP8.5 represents a scenario with a significant level of radiative forcing (nearly double the RCP4.5), falling within the 90th percentile of the reference emissions range for energy and industry carbon dioxide emissions (Moss et al. 2010). While now considered to be highly improbable, RCP8.5 is widely used since changes are most evident in this scenario (i.e., the signal-to-noise ratio is maximized) and provides a mode of comparison with both previous studies and for RCP4.5 used herein.

Daily precipitation amounts analyzed herein are derived from the Air Force Weather Agency (AFWA; Creighton et al. 2014) total simulation precipitation accumulation variable archived at 15-minute output intervals (in mm). The AFWA total precipitation variable is based on accumulation since the simulation start (Creighton et al. 2014). Daily precipitation (1200–1200 UTC) climatologies are then aggregated from the HIST, EOC4.5, and EOC8.5 15-minute sub-daily AFWA total precipitation data.

b. PRISM

To compare HIST daily extreme precipitation to observations, we use the Parameter-elevation Regressions in Independent Slopes Model (PRISM; Daly et al. 1994). PRISM data encompasses the CONUS with horizontal grid spacing of 4 km. Data are daily (1200–1200 UTC) and generated from a digital elevation model, station data (including federal, state, and local weather networks), and radar precipitation estimates (where available) to produce gridded daily precipitation estimates (Daly et al. 1994). PRISM is not ground truth per se; rather, it serves as a tool to assess the similarity between the simulated HIST and a dataset established using observations in its creation. PRISM does have disadvantages, such as limited station density and temporal inconsistencies in some regions (Daly et al. 2021); however, advantages include relatively high-resolution, quality-controlled data that are more useful in mountainous regions compared to station data alone as the process considers physiographic features (e.g., coastline proximity, topographic indices, location) to better represent areas with complexities such as precipitation shadows and temperature inversions (Daly et al. 2008; Daly et al. 2021).

Accepted for publication in *Journal of Applied Meteorology and Climatology*. DOI 10.1175/JAMC-D-23-0206.1.

PRISM data from 1 October 1990–30 September 2005 (i.e., the HIST climate simulation period) was bilinearly regridded to match the WRF-ARW lambert conformal projection and horizontal grid spacing of 3.75 km for comparison. The time series was aggregated into seasonal and annual climatologies to assess the HIST epoch performance since a one-to-one event comparison cannot be implemented due to the HIST epoch driven by a free-running GCM using historical initial conditions. To determine any error in the WRF historical baseline, we compared the HIST and PRISM output using Pearson's correlation coefficient (r), root mean square error (RMSE), and p-value (95% confidence level) from a Mann–Whitney U test for the medians using a field significance false discovery rate of α=0.1. Additionally, we chose eight climatologically unique CONUS cities for further analysis following Gensini et al. (2023): Albany, New York; Amarillo, Texas; Grand Junction, Colorado; Minneapolis, Minnesota; Nashville, Tennessee; Phoenix, Arizona; Seattle, Washington; and Tallahassee, Florida. These cities are within eight of the nine NCEI climate regions and six of the seven National Climate Assessment (NCA) CONUS regions (Karl and Kloss 1984; Wuebbles et al. 2017), thus representing a selection of climatologically diverse areas. Additionally, cities represent higher socioeconomic risk due to increased population density and vulnerabilities associated with urban infrastructure (e.g., Lee et al. 2016, Zhou et al. 2019).

c. Defining extreme precipitation

Extreme precipitation changes over relatively short intervals are particularly important due to their potential societal impacts, and given the many options, it was important to choose the optimal definition that can be directly compared to previous research and ensure relevance to those impacts. Annual extreme events can be used to determine the probability of 100-year return period precipitation values, which can then inform infrastructure design and mitigation efforts (Min et al. 2011; Wright et al. 2021). The leading definition for extreme precipitation over time interval N uses percentiles, especially above the 95th (e.g., Groisman et al. 2005; Sillmann and Roeckner 2008; O'Gorman 2012; Agel et al. 2015; Armal et al. 2018; Howarth et al. 2019). Some studies have used multiple thresholds of percentiles to show changes in various parts of the probability density function (e.g., Groisman et al. 2005; Alexander et al. 2006; Allan and Soden 2008; Loiraux et al. 2013; Huang and Stevenson 2021). Here, we define extreme daily precipitation to be the 99th percentile of daily precipitation over the entire epoch time series. 24-h all-day percentiles are

Accepted for publication in *Journal of Applied Meteorology and Climatology*. DOI 10.1175/JAMC-D-23-0206.1.

used over wet-day percentiles, as the latter can produce misleading results due to high sensitivity to the fraction of wet days and precipitation accumulations of a day or longer are relevant for areal flooding (e.g., Lenderink and van Meijgaard 2008; O'Gorman and Schneider 2009; Min et al. 2011; Chan et al. 2014; Agel et al. 2015; Schär et al. 2016; Armal et al. 2018; Changnon and Gensini 2019).

d. Extreme Value Analysis (EVA)

Extreme value theory (EVT; Gumbel 1958) characterizes the frequency and intensity of extremes (e.g., Friederichs 2010; Min et al. 2011; Kunkel et al. 2013a; Westra et al. 2013; Agel et al. 2015; Kumar et al. 2015; Tabari 2021; Gensini et al. 2023). EVT is useful since extremes would stay constant in a stationary climate, but revealing a trend indicates attribution to nonstationary forcing, such as anthropogenic climate change. Here, we implement univariate EVA using the Fisher-Tippett-Gnedenko (Fisher and Tippett 1928; Gnedenko 1943) theorem with the daily precipitation time series for the PRISM, HIST, EOC4.5, and EOC8.5 epochs and performed the analysis with the Python package pyextremes (https://georgebv.github.io/pyextremes/) inspired by Coles (2001).

The generalized extreme value approach has two methods for analysis: block maxima (BM) and peak over threshold (POT). With a block size of one year, the BM method takes the maximum value from each year, making the sample size equal to the number of years. The POT method permits a larger sample size by extracting events based on a selected critical value but is highly dependent on the critical threshold value chosen and can result in misleading conclusions (Friederichs 2010; Tabari 2021). In comparing BM and POT methods for climate change impacts on global flood and extreme precipitation events, Tabari (2021) found the difference in magnitude between the methods to be statistically significant for longer return intervals; spatially, these methods displayed inconsistency in the tropics and subtropics, yet high consistency in the Northern Hemisphere extratropics. Here, we use the BM technique since it creates a more stable model, whereas POT is highly dependent on the threshold chosen and clustering distance, making the model more sensitive. To avoid capturing seasonality, we chose a BM block size of one year and extracted values for the model based on the maximum 24-h precipitation value for each hydrologic year (totaling 15 values for each epoch).

Extracted extremes were fit to a maximum likelihood estimate model and a right-skewed Gumbel distribution. The right-skewed Gumbel distribution was selected using model metrics

Accepted for publication in *Journal of Applied Meteorology and Climatology*. DOI 10.1175/JAMC-D-23-0206.1.

of Akaike Information Criterion (AIC), log-likelihood, location, and scale to compare the right-skewed Gumbel and generalized extreme distribution fits on the extracted time series. AIC uses log-likelihood in the calculation and evaluates how accurately the modeled EVA data fits the original WRF input to compare the relative goodness-of-fit; a lower score indicates better modeled data. The AIC for all epochs in each city showed that the right-skewed Gumbel distribution had lower scores than the generalized extreme value distribution, except for the HIST and EOC8.5 epochs for Seattle, WA (Fig. 3 in Stinnett 2023).

Quantile-Quantile (Q-Q) plots for the cities have the same *x* and y-axis scale to compare the modeled EVA and input WRF data to establish the accuracy of the modeled data, which is linear on a 1:1 trend line when the modeled EVA data reasonably describes the original input WRF data input. Model statistics such as Pearson's *r*, RMSE, *p*-value, and coefficient of determination (R^2) were used to rate model performance. R^2 demonstrates how well the modeled EVA values match the WRF input by explaining the variance from the input WRF data and is the better model reliability metric. This metric contrasts Pearson's *r* which evaluates only the distribution pattern but helps compare the historical baseline with independent observations since it is not a one-to-one comparison like used in the EVA. Probability density functions (PDFs) were calculated for all four epochs (PRISM, HIST, EOC4.5, and EOC8.5). These PDFs are of the modeled extremes, not the entire epoch time series, where each point has a value and associated probability to further identify variability within the epochs.

The probability of exceedance (*P*) is the probability of a value with a specific rank being exceeded within the given time period. *P* is calculated using the equation:

$$P = \frac{r - \alpha}{n + 1 - \alpha - \beta}$$

where *r* is the rank of the extreme value, *n* is the number of extreme values, and α and β are empirical plotting parameters. EVA utilizes the Weibull plotting position where α=0 and β=0. For the extracted data used here, rank values are from 1–15 where the most extreme value has a rank of 1 and the annual exceedance probability is 1/16 or 0.0625.

The return period (*R*; Makkonen 2006) relates to the likelihood of a precipitation value occurring within any given year. *R* is calculated following:

$$R = \frac{1}{P\lambda}$$

File generated with AMS Word template 2.0

Accepted for publication in *Journal of Applied Meteorology and Climatology*. DOI 10.1175/JAMC-D-23-0206.1.

where P is the annual probability of exceedance (i.e., 1% for a 100-year event) and λ is the rate of extreme events per block which equals 1 with a return period and block size of one year. We used a 1,000-iteration bootstrap sample to calculate the 95% confidence interval of the 2–500-year return periods. Statistical significance was determined where the median EOC epoch return period precipitation value was outside the 95% confidence interval from the 1000-iteration bootstrap sample for the HIST. A wider confidence interval signifies higher uncertainty, partly due to a limited amount of input data, which is a limitation in the return period calculations for these datasets.

The spatial plots of the 100-year return periods of daily precipitation values for the eight climatologically unique cities were spatially aggregated to 30 km from the native 3.75 km horizontal grid spacing using both a spatial mean and a spatial maximum to account for spatial uncertainty. The HIST 30 km mean return period daily precipitation values were closest to NOAA ATLAS 14 series (e.g., Vol. 9; Perica et al. 2013 and Vol. 10; Perica et al. 2015, revised 2019), PRISM, and the native grid spacing data compared to the HIST 30 km max (not shown). Therefore, we continued to use the 30 km mean value in the spatial analysis of the EOC4.5 and EOC8.5 100-year return interval to reduce computational expense.

3. Results

a. Comparison of HIST to PRISM

Despite a few regional and seasonal biases, HIST daily mean and extreme precipitation compared favorably to PRISM. Pearson's r correlation for average annual precipitation between PRISM and HIST was found to be 0.89 herein and 0.91 in Gensini et al. (2023), while the RMSE was found to be 214.6 mm herein and 210 mm in Gensini et al. (2023) (Table 1). These differences between the current study and Gensini et al. (2023) are likely associated with differing regridding and spatial clipping techniques used on the time series domain. The annual 99th percentiles of PRISM and HIST were also highly correlated with a Pearson's r correlation of 0.89, $p \approx 0$, and RMSE = 7.8 mm (Fig. 1a–d and Table 1). Pearson's r correlation between PRISM and HIST minimally dropped for the 99th percentile seasonally (Dec–Feb = 0.89; Mar–May = 0.87; Jun–Aug = 0.88; Sep–Nov = 0.84) compared to seasonal mean precipitation (Table 1). These model metrics illustrate that HIST admirably represented the mean and 99th percentile of daily precipitation annually and seasonally compared to PRISM.

Accepted for publication in *Journal of Applied Meteorology and Climatology*. DOI 10.1175/JAMC-D-23-0206.1.

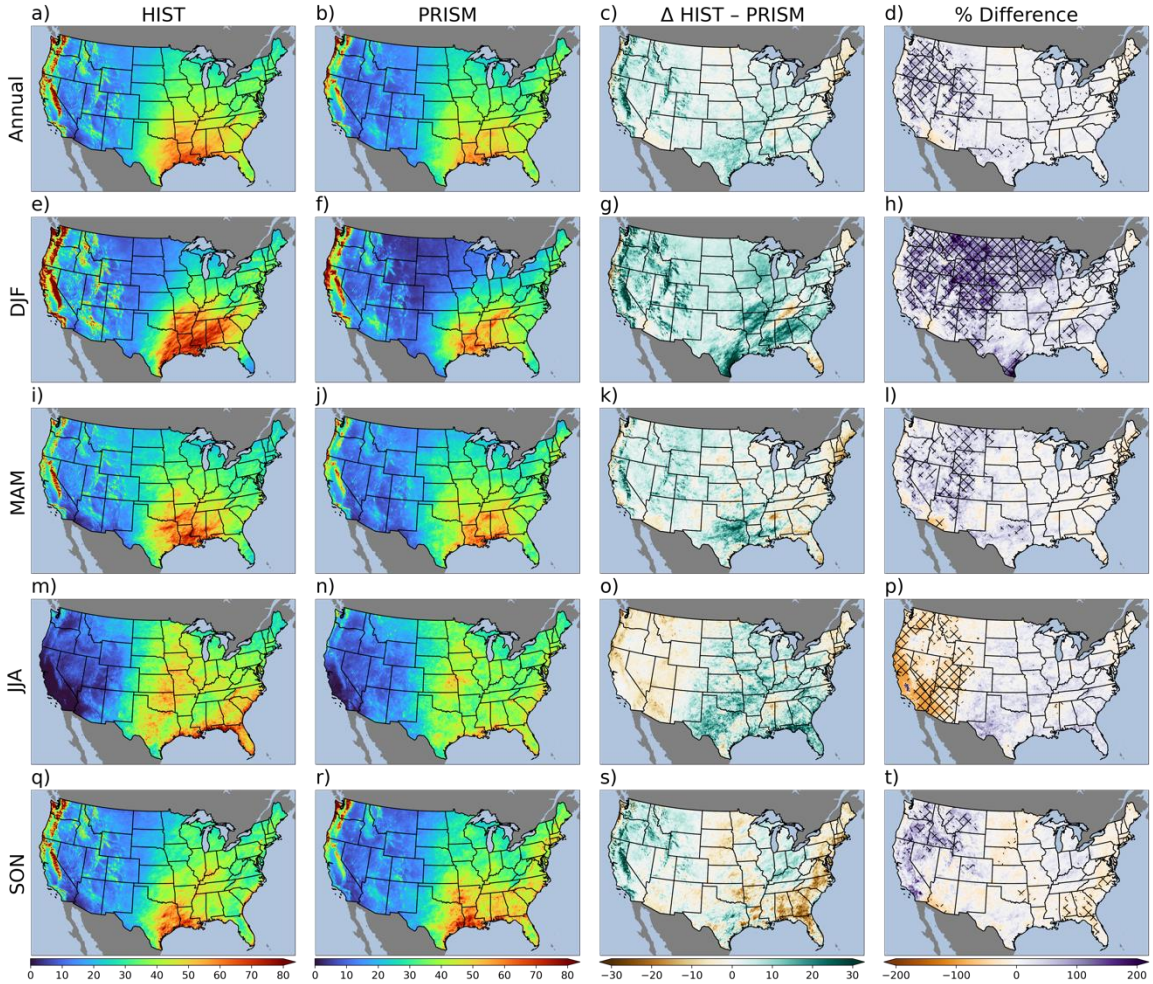

Fig. 1. 99th percentile of daily precipitation (mm) for 1990–2005 HIST (a, e, i, m, q) and PRISM (b, f, j, n, r), and the raw (c, g, k, o, s) and percent differences (d, h, l, p, t) between them for annual (first row), Dec–Feb (second row), Mar–May (third row), Jun–Aug (fourth row), and Sep–Nov (fifth row). Root mean square error values for each row are shown in Table 1. Hatched areas in the fourth column indicate where a Mann–Whitney *U* test determined statistically significant differences ($p < 0.05$) between the epochs with a field significance false discovery rate of α=0.1.

	Mean Precipitation				
	Annual	**DJF**	**MAM**	**JJA**	**SON**
r	0.89	0.91	0.87	0.90	0.84
p	0.0	0.0	0.0	0.0	0.0
RMSE	214.6	87.3	58.4	77.9	68.9
	Daily 99th Percentile				
	Annual	**DJF**	**MAM**	**JJA**	**SON**
r	0.89	0.89	0.87	0.88	0.84
p	0.0	0.0	0.0	0.0	0.0
RMSE	7.8	12.3	7.9	9.2	8.9

Accepted for publication in *Journal of Applied Meteorology and Climatology*. DOI 10.1175/JAMC-D-23-0206.1.

Table 1. Comparison of 1990–2005 PRISM and HIST mean and daily 99th percentile precipitation.

Regarding regional biases, the HIST annual 99th percentile of daily precipitation was significantly wetter for a large area of the Intermountain West and smaller areas in the southern Great Plains and Midwest, while significantly drier areas were mainly confined to the Northeast (Fig. 1d). On a seasonal basis, there were differences in the magnitude of the 99th percentile of daily precipitation for various regions with raw differences primarily within 20 mm; each season had an RMSE of 12.3 (Dec–Feb), 7.9 (Mar–May), 9.2 (Jun–Aug), and 8.9 (Sep–Nov) mm. Differences between HIST and PRISM displayed a statistically significant ($p < 0.05$) wet bias in regions of Intermountain West during Sept–Feb and in the northern Great Plains and Midwest during Dec–Feb (Fig. 1h, t). Some of these regions coincided with less than 10 mm raw differences—especially in the northern Great Plains—but made for large percent (e.g., +150%) differences due to relatively small denominators. Similarly, the statistically significant HIST dry bias in the western CONUS for Jun–Aug (Fig. 1p) also showed small absolute differences and large negative percent differences (i.e., HIST underestimated precipitation). As suggested in Gensini et al. (2023), this dry bias could be partly related to the North American Monsoon season, which peaks in the warm season for the Southwest (Adams and Comrie 1997). The Sep–Nov statistically significant dry bias in the Southeast and along the Atlantic coast may be attributed to poor model representation of tropical cyclone precipitation due to limited model domain extent over the Gulf of Mexico and Atlantic Ocean (Figs. 1s, t). It is important to note that caution should be used when interpreting PRISM as ground truth during analysis since it has limitations, especially in regions with limited station density and radar coverage.

b. Future changes in percentiles

We compared HIST to potential future climate scenarios (EOC; 2085–2100) using RCP4.5 (EOC4.5) and RCP8.5 (EOC8.5) to assess future changes in extreme precipitation. In HIST, the daily 99th percentile precipitation values were generally less than 80 mm for most CONUS locations. A pattern emerged in both EOC scenarios across seasons, which showed the highest magnitude changes in the 99th percentile of daily precipitation were increases in the Cascade Mountains and Ohio River Valley and decreases in the Southwest and southern Great Plains (Figs. 2, 3, 4, 5). These changes align with previous research examining historical and potential future changes for percentiles in these regions of the CONUS (e.g.,

Accepted for publication in *Journal of Applied Meteorology and Climatology*. DOI 10.1175/JAMC-D-23-0206.1.

Groisman et al. 2005; Alexander et al. 2006; Kunkel et al. 2013a; Janssen et al. 2014; Huang et al. 2017; Fowler et al. 2021; Huang and Stevenson 2021). Part of the projected increases in annual precipitation (Gensini et al. 2023) could be explained by an increase in the 99th percentile values in the future, which indicates an increasing probability of extreme precipitation (i.e., exceeding the HIST 99th percentile) by the end of the twenty-first century in both EOC scenarios.

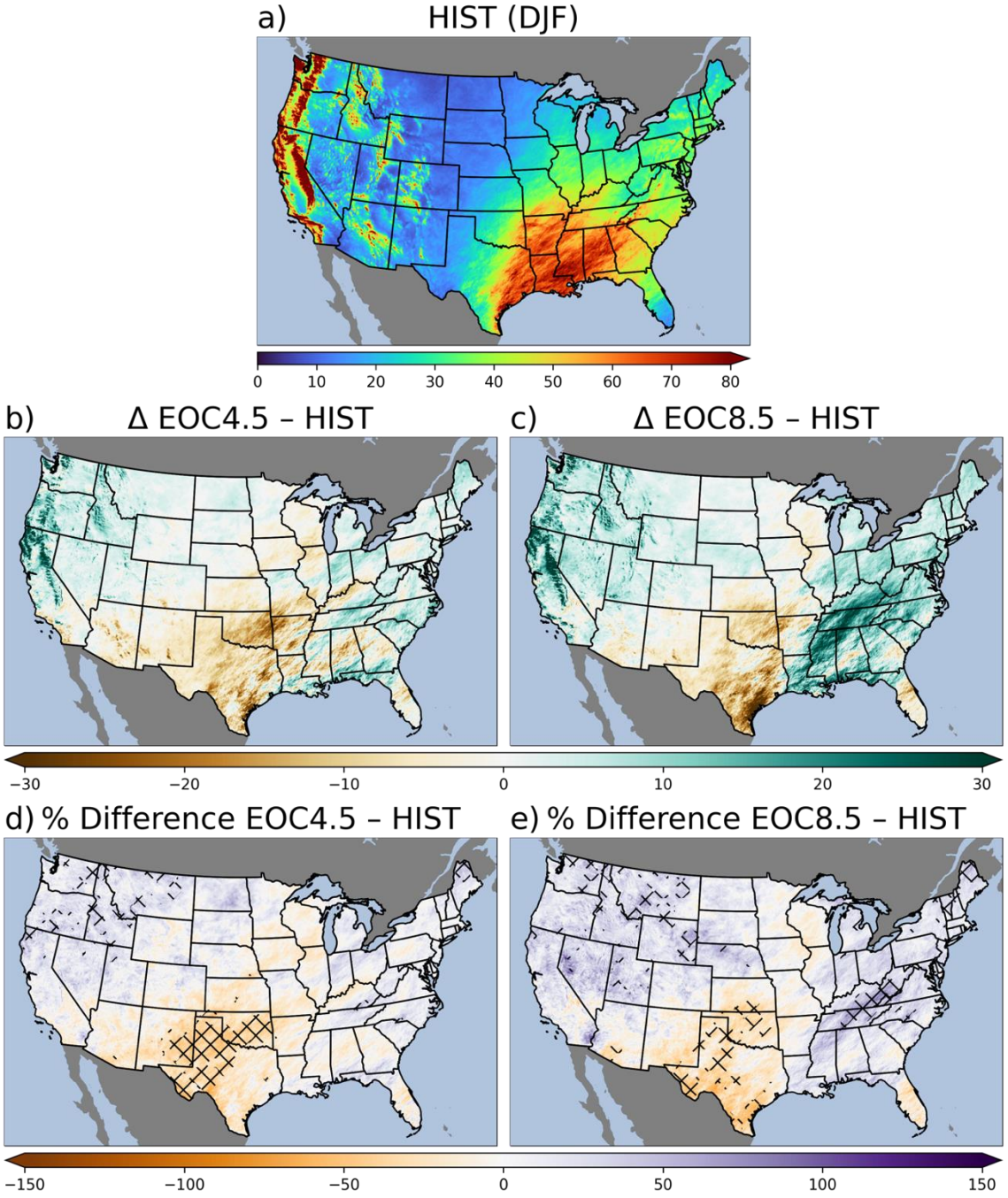

Fig 2. Dec–Feb 99th percentile of daily precipitation (mm) for 1990–2005 HIST (a), with raw (b, c) and percent (d, e) differences from HIST for 2085–2100 EOC4.5 and EOC8.5

Accepted for publication in *Journal of Applied Meteorology and Climatology*. DOI 10.1175/JAMC-D-23-0206.1.

epochs. Hatched areas on percent difference panels (third row) indicate regions where a Mann–Whitney *U* test determined statistically significant differences ($p < 0.05$) between the epochs with a field significance false discovery rate of α=0.1.

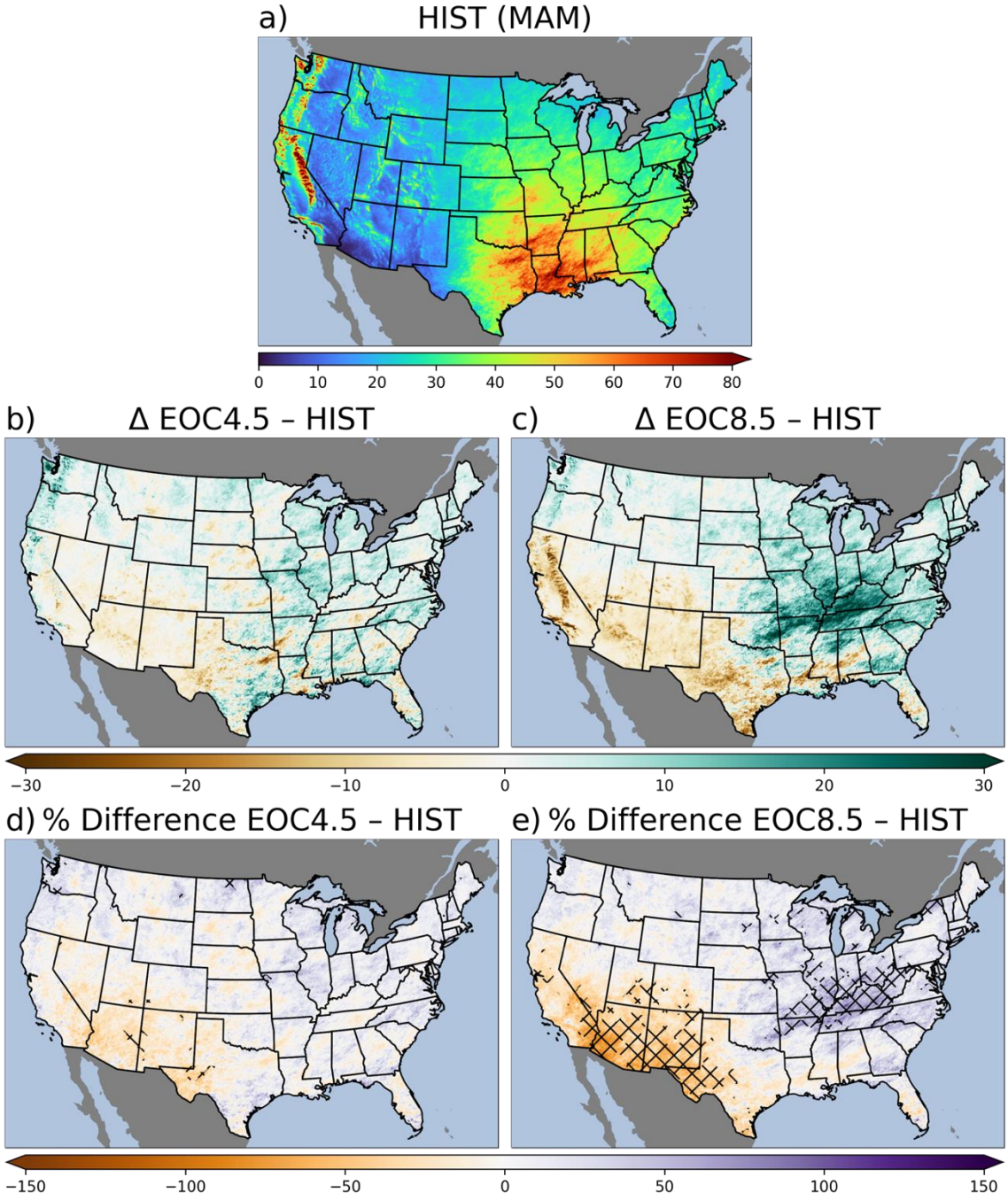

Fig. 3. As in Fig. 2, except for Mar–May.

File generated with AMS Word template 2.0

Accepted for publication in *Journal of Applied Meteorology and Climatology*. DOI 10.1175/JAMC-D-23-0206.1.

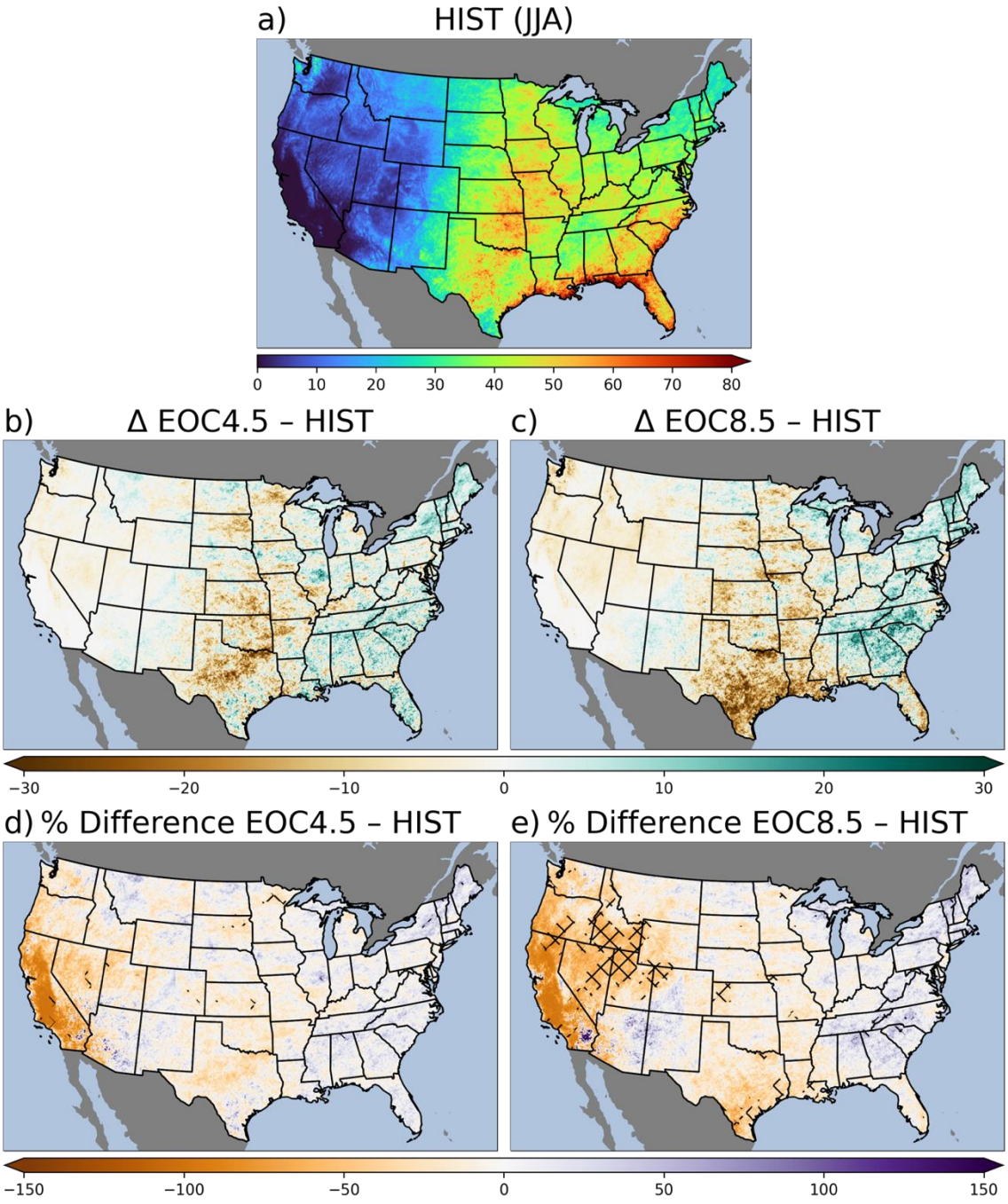

Fig. 4. As in Fig. 2, except for Jun–Aug.

Accepted for publication in *Journal of Applied Meteorology and Climatology*. DOI 10.1175/JAMC-D-23-0206.1.

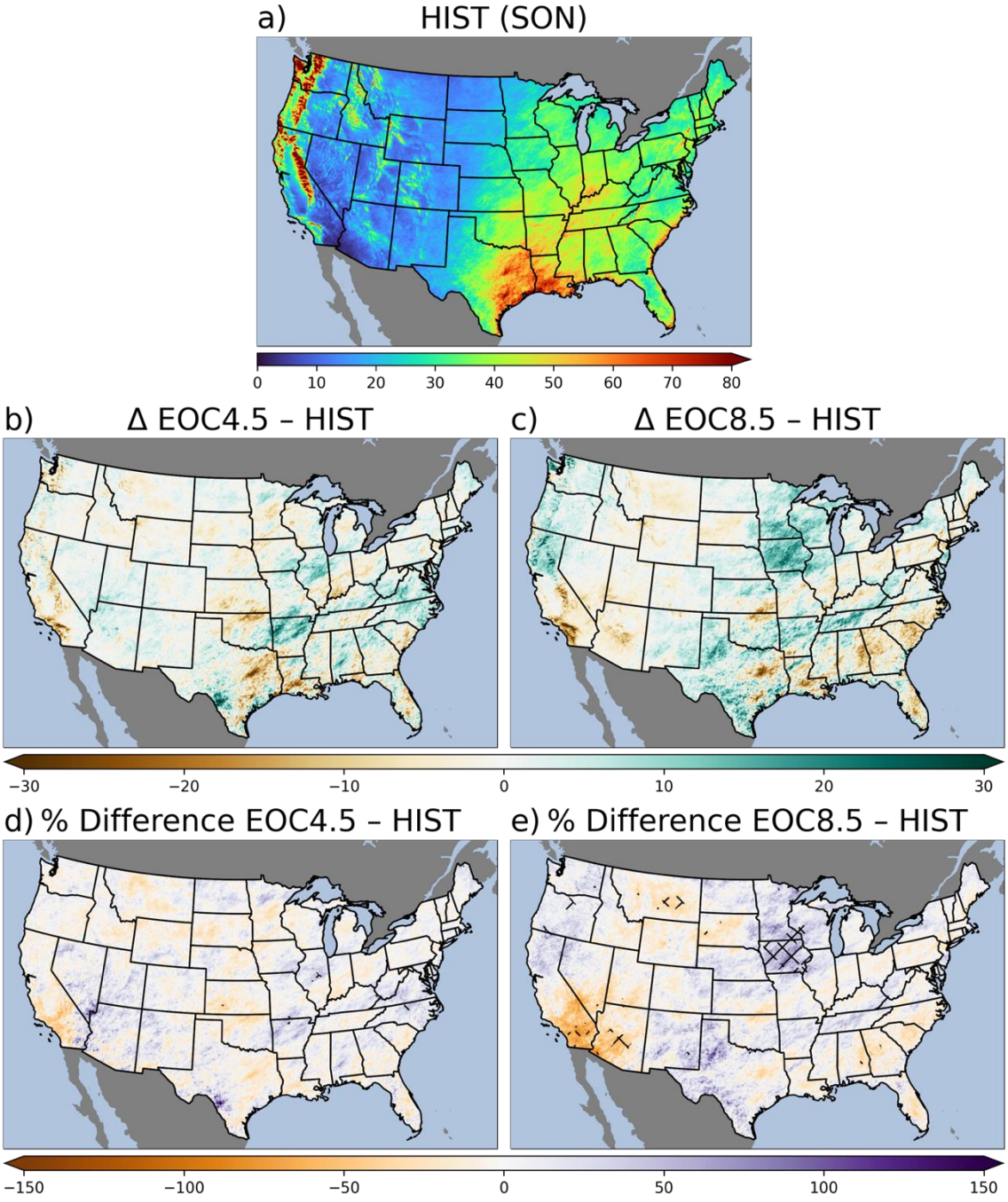

Fig. 5. As in Fig. 2, except for Sep–Nov.

1) WESTERN CONUS

Implementing a seasonal analysis of the 99th percentile of daily precipitation permits the identification of specific spatiotemporal changes through the end of the twenty-first century. Results reveal the largest areas of statistically significant decreases in the 99th percentile of daily precipitation were in EOC8.5 in the Southwest (Mar–May; Fig. 3e) and Intermountain West (Jun–Aug; Fig. 4e). Most of these areas of decrease in the 99th percentile of daily

Accepted for publication in *Journal of Applied Meteorology and Climatology*. DOI 10.1175/JAMC-D-23-0206.1.

precipitation are consistent with statistically significant decreases in mean seasonal precipitation in EOC8.5 as compared to HIST (Gensini et al. 2023). Many decreases in the 99th percentile of daily precipitation had large negative percent differences of 50–150% in the Southwest and Intermountain West, consistent with the recent drought trends in these regions and previous work projecting increasing aridity through the end of the twenty-first century (e.g., Mishra and Singh 2010; Dai 2011; Naumann et al. 2018; Cook et al. 2020; Ukkola et al. 2020). Therefore, changes in extreme precipitation in these regions will have large implications for regional hydroclimate stability and water scarcity in these climatologically arid regions.

Smaller, more sporadic regions of the northern Intermountain West displayed statistically significant increases of the 99th percentile of daily precipitation for both EOC scenarios in Dec–Feb (Fig. 2d, e), and EOC8.5 mean seasonal precipitation during Dec–May showed statistically significant increases in the Pacific Northwest (Gensini et al. 2023). Assuming the 0°C isotherm remains low in elevation, the differences between the EOC scenarios and HIST could imply an increased ceiling for snowpack in mountainous areas of the western CONUS, especially in the Pacific Northwest. However, Gensini et al. (2023) show temperature increases of approximately 2–7°C in areas of the Intermountain West during Dec–Feb EOC8.5 compared to HIST, while Mar–May exhibit less than 2°C of warming for most regions of the Intermountain West. Thus, the potential change of a smaller fraction of precipitation falling as snow could lead to an increased flood risk during winter and spring and water scarcity in summer due to decreased snowpack (Pan et al. 2011; Trenberth 2011; Li et al. 2022; Asif et al. 2023). These results agree with previous simulations encompassing the western CONUS projecting precipitation increases, most notably in the Pacific Northwest, by the end of the twenty-first century (e.g., Pan et al. 2011; Dominguez et al. 2012; Huang and Stevenson 2021).

2) Eastern CONUS

The eastern CONUS (i.e., regions east of the Rocky Mountains) showed the highest 99th percentile of daily precipitation in the Midwest and Southeast in all seasons (Figs. 2, 3, 4, 5). Mean seasonal precipitation in the southern Great Plains in Dec–Feb showed statistically significant decreases in EOC8.5 compared to HIST (Gensini et al. 2023). Similarly, the 99th percentile of daily precipitation displayed areas of statistically significant decreases in the southern Great Plains during Dec–Feb (EOC4.5 and EOC8.5; Fig. 2d, e) and Mar–May

Accepted for publication in *Journal of Applied Meteorology and Climatology*. DOI 10.1175/JAMC-D-23-0206.1.

(EOC8.5; Fig. 3e). No widespread statistically significant changes were seen for EOC4.5 in Mar–Nov (Figs. 3d, 4d, and 5d), but raw differences showed widespread decreases in the Great Plains, Midwest, and Mid-South for Jun–Aug in both EOC scenarios (Fig. 4b, c).

The climatological peak for tropical cyclones—one source of extreme precipitation—occurs during Sept–Nov, with 70% and 58% of extreme precipitation events resulting from tropical cyclones in September and October, respectively, during the period 2002–2011 (e.g., Kunkel et al. 2012; Stevenson and Schumacher 2014; Moore et al. 2015). Our simulations showed large areas of decrease in the Southeast and Atlantic Coast during Sep–Nov in EOC4.5 and EOC8.5 (Fig. 5b, c) but small areas of statistical significance (Fig. 5d, e). These projected changes could be due to decreased tropical cyclone frequency and related precipitation. However, since the HIST showed a statistically significant dry bias for those regions during Sep–Nov (Fig. 1t), extreme precipitation caused by tropical cyclones may be underestimated in the HIST and EOC simulations.

EOC8.5 seasonal mean precipitation in the Midwest and Ohio Valley had statistically significant increases in Mar–May (Gensini et al. 2023). These regions also displayed widespread robust statistically significant increases of up to 100% for the 99th percentile of daily precipitation during Sep–May in EOC8.5 (Figs. 2e, 3e, 5e). The largest area of increase transitions from the lower Midwest and Ohio Valley in Dec–May to the upper Midwest in Sep–Nov. Historically, mean MCS precipitation during the warm season is focused across the Midwest and central Great Plains, with large percentages of annual precipitation falling within this time (e.g., Ashley et al. 2003; Schumacher and Johnson 2006; Stevenson and Schumacher 2014; Feng et al. 2016; Prein et al. 2017; Haberlie and Ashley 2019). For example, the Midwest and central Great Plains experienced 350–400 mm of MCS precipitation during May–Aug, accounting for upwards of 50–60% of annual accumulation (Haberlie and Ashley 2019). The most robust statistically significant increases in mean MCS precipitation are in the Northeast into the Appalachian Mountains (Jun–Aug), Ohio Valley (Dec–May), and Midwest (Mar–May and Sep–Nov) (Haberlie et al. 2023). These regions closely resemble the areas of significant increase in the 99th percentile of daily precipitation presented here and experience an increase in average MCS precipitation of approximately 100–150+ (50) mm in Dec–May EOC8.5 (EOC4.5) as compared to HIST (Haberlie et al. 2023). Precipitation in the Southeast, Midwest, and Northeast CONUS has increased historically and has the potential to be further exacerbated by anthropogenic climate change

Accepted for publication in *Journal of Applied Meteorology and Climatology*. DOI 10.1175/JAMC-D-23-0206.1.

(Groisman et al. 2005; Alexander et al. 2006; Groisman et al. 2012; Kunkel et al. 2013a; Janssen et al. 2014; Huang et al. 2017; Changnon and Gensini 2019; Howarth et al. 2019; Fowler et al. 2021). Overall, the 99th percentile of daily precipitation displayed large areas of greater than 50% increase by the end of the twenty-first century in all seasons except Jun–Aug (Figs. 2, 3, 4, 5). These increases in the 99th percentile of daily precipitation are particularly concerning given the numerous high-impact floods affecting those regions in recent decades (e.g., Junker et al. 1999; Lackmann 2013; Zhang and Villarini 2017; Kraft et al. 2023).

c. Extreme value analysis

Q–Q plots indicate the goodness of fit for the input WRF time series and modeled EVA distributions (Fig. 6). All cities showed reasonable estimations for the modeled extremes at lower magnitudes and transition to underestimating at the highest magnitudes in six of the eight cities (Fig. 6a, b, c, e, g, h). Estimation bias may be due to extracted extremes being skewed within the upper tail of the distribution, and there are still significant outliers when extracting just the extremes of the dataset. Bias is illustrated in the Albany EOC8.5 and Tallahassee HIST epochs, where the difference between the highest magnitude and the third highest magnitude extracted values is approximately 100 mm (Fig. 6a, h). Therefore, when the difference between the largest extreme values is high in magnitude, there is more underestimation by the model for those upper values, but the other lower magnitude values displayed good estimation by the model. The estimation bias is also shown in Grand Junction EOC4.5 and Seattle EOC8.5 (Fig. 6c, g). The larger magnitude values are affected by an estimation bias partly due to the small amount of input data (15 values); however, doubling the input data to 30 values (block size of 6 months instead of 12 months) still displayed these estimation biases at the highest magnitudes.

Accepted for publication in *Journal of Applied Meteorology and Climatology*. DOI 10.1175/JAMC-D-23-0206.1.

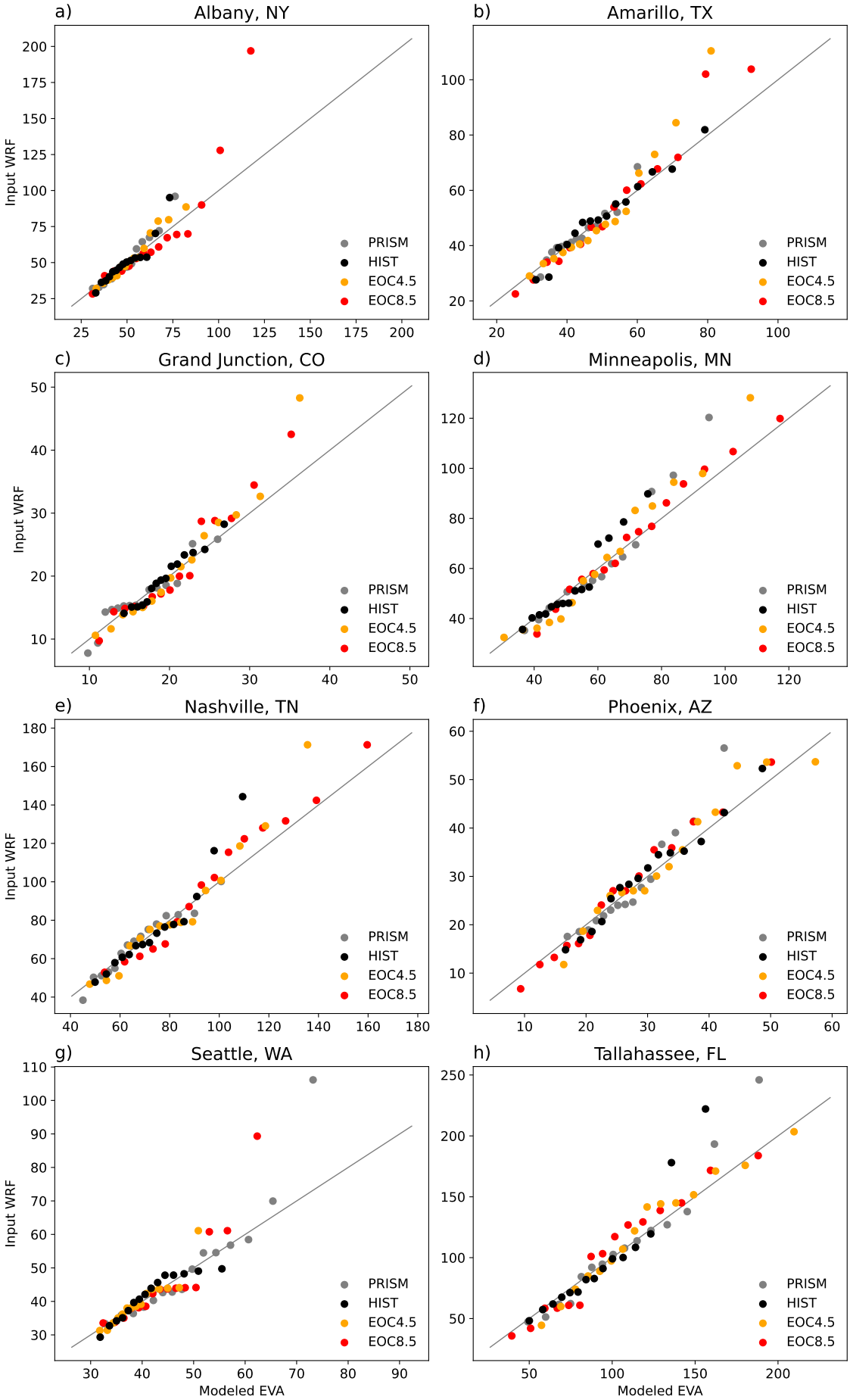

Accepted for publication in *Journal of Applied Meteorology and Climatology*. DOI 10.1175/JAMC-D-23-0206.1.

Fig. 6. Q-Q plot of the input WRF versus modeled EVA daily precipitation (mm) extreme values for 1990–2005 PRISM (grey) and HIST (black), and 2085–2100 EOC4.5 (orange) and EOC8.5 (red) epochs with a block size of one year resulting in 15 values for eight climatologically unique cities. The solid line shows the 1:1 trend line, and dots show the values of the modeled EVA (*x* axis) and input WRF (*y* axis) data.

Model metrics of *r*, *p*, RMSE, and R^2 represent the empirical relationship between the modeled EVA and input WRF distributions. Reasonable model estimation of the input simulation data is shown with lower values of *p* and RMSE, while *r* and R^2 require a value closer to one. RMSE values for each city were relatively low considering the limited number of input extreme values and the underestimation at high precipitation values for some epochs (Table 2). For example, Tallahassee HIST had an RMSE of 20 mm, but only the two highest magnitude values of HIST were underestimated which led to a higher overall RMSE even though all other lower magnitude values had reasonable model estimation (Fig. 6h and Table 2). The RMSE is skewed by those two highest magnitude precipitation values being more robustly underestimated and using the Q-Q plot gives the visual representation that the other 13 modeled values performed well (Fig 6h). Similarly, an underestimation bias is seen for Albany EOC8.5 and Seattle EOC8.5 (Fig. 6a, g and Table 2). The *p*-values for all cities were approximately zero and Pearson's *r* showed high correlation with all cities greater than 0.9, with most epochs greater than 0.95 (Table 2). While Pearson's *r* shows admirable correlation in the distribution patterns of the modeled EVA and input WRF data, R^2 displays good model reliability with values greater than 0.85, indicating that HIST explained at least 85% of the variance from the input data for most epochs in each city. Using these statistical model metrics in combination with the Q–Q plots gives confidence in the reliability of the modeled EVA extremes from the input WRF data used in the proceeding EVA analysis.

Accepted for publication in *Journal of Applied Meteorology and Climatology*. DOI 10.1175/JAMC-D-23-0206.1.

	PRISM	HIST	EOC4.5	EOC8.5
			Albany, NY	
r	0.977	0.939	0.985	0.908
p	0.000	0.000	0.000	0.000
RMSE	6.022	6.238	4.686	22.237
R^2	0.877	0.831	0.924	0.704
			Amarillo, TX	
r	0.968	0.985	0.962	0.982
p	0.000	0.000	0.000	0.000
RMSE	2.730	2.608	9.109	6.875
R^2	0.920	0.966	0.821	0.915
			Grand Junction, CO	
r	0.950	0.986	0.976	0.973
p	0.000	0.000	0.000	0.000
RMSE	1.440	0.905	3.362	2.910
R^2	0.903	0.949	0.879	0.889
			Minneapolis, MN	
r	0.971	0.964	0.986	0.994
p	0.000	0.000	0.000	0.000
RMSE	8.504	6.067	7.822	3.868
R^2	0.859	0.846	0.918	0.973
			Nashville, TN	
r	0.975	0.952	0.973	0.989
p	0.000	0.000	0.000	0.000
RMSE	3.530	10.473	10.852	7.611
R^2	0.950	0.815	0.887	0.951
			Phoenix, AZ	
r	0.964	0.987	0.971	0.993
p	0.000	0.000	0.000	0.000
RMSE	4.286	1.922	3.205	2.448
R^2	0.831	0.962	0.934	0.964
			Seattle, WA	
r	0.928	0.937	0.937	0.905
p	0.000	0.000	0.000	0.000
RMSE	8.786	2.273	2.897	7.688
R^2	0.756	0.874	0.832	0.701
			Tallahassee, FL	
r	0.972	0.947	0.982	0.975
p	0.000	0.000	0.000	0.000
RMSE	17.702	20.572	8.892	11.307
R^2	0.882	0.793	0.960	0.939

Table 2. Metrics of the modeled EVA and input WRF data for 1990–2005 PRISM and HIST, and 2085–2100 EOC4.5 and EOC8.5 epochs for eight climatologically unique cities.

Accepted for publication in *Journal of Applied Meteorology and Climatology*. DOI 10.1175/JAMC-D-23-0206.1.

We used PDFs to detect the variability of the extreme daily precipitation values in the epochs from extreme precipitation values extracted for the EVA. Amarillo and Grand Junction are the only cities where HIST exceeds PRISM in the upper tail of the PDF (Fig. 7b, c). Differences are expected based on the limitations of using PRISM as the observational dataset for comparison to HIST, especially in mountainous and climatologically arid regions of the CONUS, which Amarillo, Grand Junction, Phoenix, and Seattle represent (Fig. 7b, c, f, g). Albany, Minneapolis, Nashville, Phoenix, and Tallahassee displayed the highest differences in the peak of the PDF curve in one or both EOC scenarios (Fig. 7a, d, e, f, h). For these cities, the decrease in the peak probability density indicates more variability and typically an increased ceiling for precipitation extremes. These scenarios have flattened PDF curves (i.e., differing probability densities at the PDF peak) with higher magnitude precipitation values at the upper tail of the distribution. The PDFs further indicate the potential for increased variability and a higher ceiling for extremes by the end of the twenty-first century.

Accepted for publication in *Journal of Applied Meteorology and Climatology*. DOI 10.1175/JAMC-D-23-0206.1.

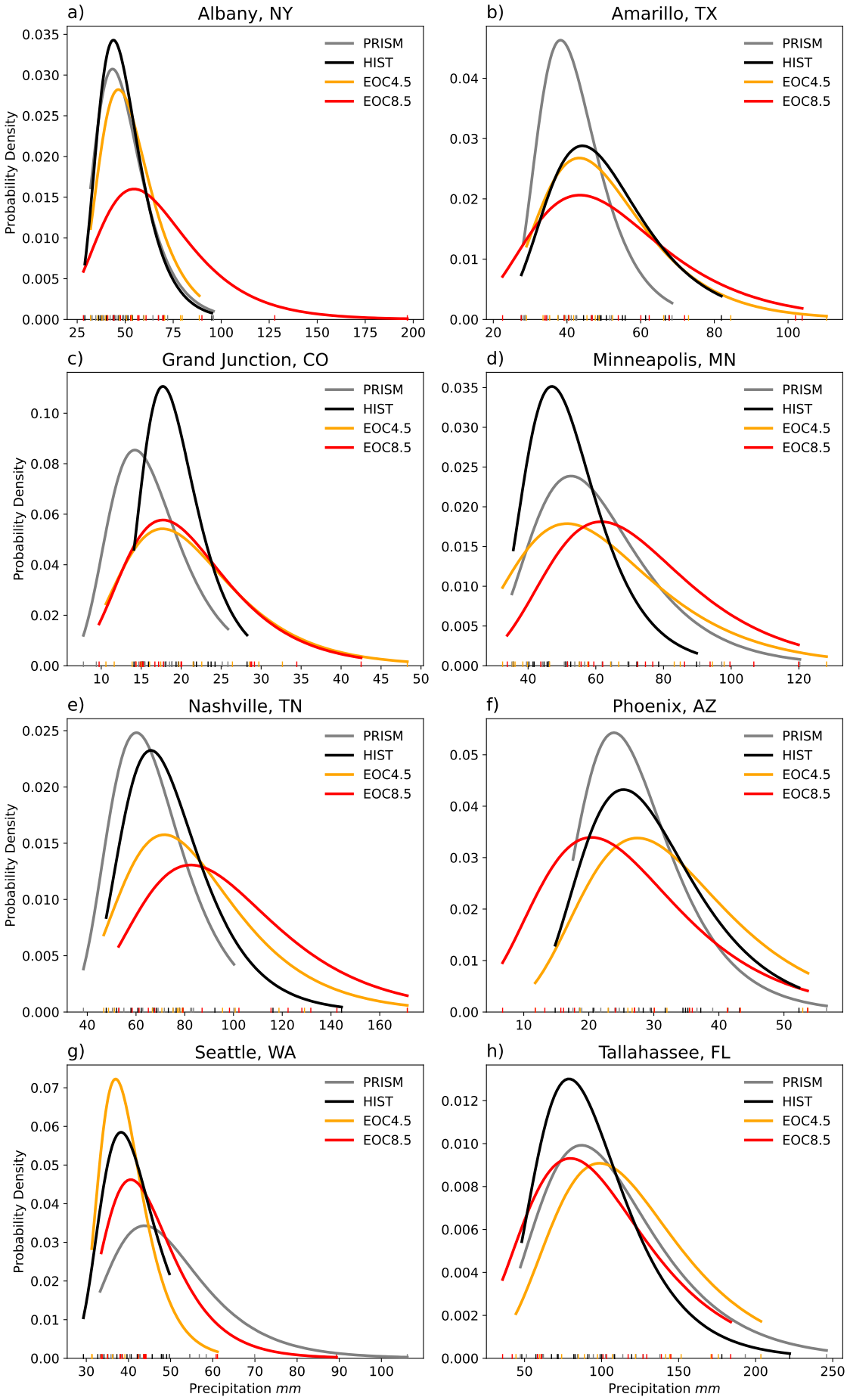

Accepted for publication in *Journal of Applied Meteorology and Climatology*. DOI 10.1175/JAMC-D-23-0206.1.

Fig. 7. The probability density (*y* axis) of daily precipitation (mm) extremes (*x* axis) for 1990–2005 PRISM (grey) and HIST (black), and 2085–2100 EOC4.5 (orange) and EOC8.5 (red) epochs simulation data for eight climatologically unique cities.

1) RETURN PERIODS

Every climatologically unique city displayed an increase over HIST in one or both EOC scenario return period daily precipitation values for 25–500 years (Fig. 8). For the comparison of PRISM and HIST, PRISM was within the 95% confidence interval of HIST for all return periods except in Amarillo and Seattle where they were below and above the 95% confidence interval, respectively (Fig. 9). Seattle EOC4.5 scenario is the only city that had an EOC scenario below HIST for all return periods examined (Figs. 8g and 9). The return period daily precipitation values for each epoch have a 95% confidence interval, which becomes large with increasing return periods since some uncertainty of the model comes from extrapolating the simulation record of 15 years to longer return periods (Figs. 8 and 9). All cities except Amarillo showed differences of less than 30% between PRISM and HIST, with many cities below 20% (i.e., Albany, Grand Junction, Nashville, Phoenix, and Tallahassee) (Fig. 9). Overall, even with some biases in HIST EOC8.5 showed the most robust increases from HIST for all return periods; EOC4.5 changes were generally lower in magnitude but still showed modest increases.

Accepted for publication in *Journal of Applied Meteorology and Climatology*. DOI 10.1175/JAMC-D-23-0206.1.

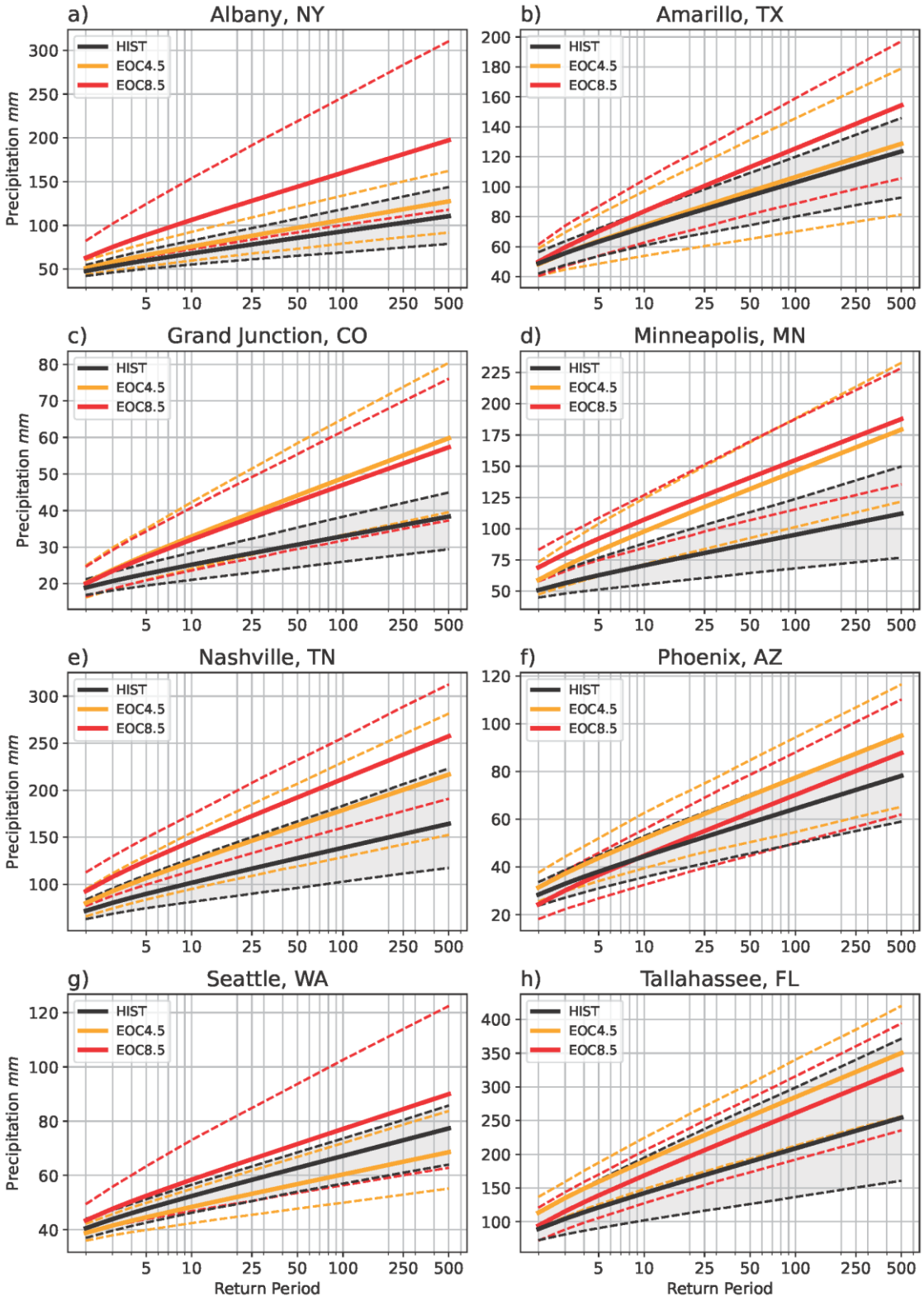

Fig. 8. Return periods (*x* axis; years) of daily precipitation (*y* axis; mm) for 1990–2005 HIST (black), 2085–2100 EOC4.5 (orange), and 2085–2100 EOC8.5 (red) epochs for eight climatologically unique cities. Solid lines denote the median modeled return period. Dashed lines indicate the 95% confidence interval (HIST is shaded) calculated using a 1000-iteration bootstrap sample.

Accepted for publication in *Journal of Applied Meteorology and Climatology*. DOI 10.1175/JAMC-D-23-0206.1.

	5		10		25		50		75		100		250		500	
Albany, NY																
PRISM	61	[61, ±12]	70	[70, ±15]	81	[81, ±20]	90	[89, ±24]	95	[94, ±26]	98	[97, ±27]	109	[108, ±32]	117	[116, ±35]
HIST	59	[61, ±10]	68	[69, ±13]	78	[79, ±17]	85	[87, ±21]	90	[92, ±23]	93	[95, ±24]	103	[105, ±28]	110	[112, ±31]
EOC4.5	66	[65, ±13]	75	[75, ±16]	88	[86, ±21]	97	[95, ±24]	102	[100, ±26]	106	[104, ±28]	118	[116, ±32]	127	[124, ±36]
EOC8.5	89	[95, ±30]	106	[115, ±40]	128	[140, ±54]	144	[159, ±64]	153	[169, ±70]	160	[177, ±74]	181	[200, ±85]	197	[218, ±95]
Amarillo, TX																
PRISM	50	[50, ±6]	56	[56, ±8]	63	[63, ±10]	69	[68, ±12]	72	[72, ±14]	74	[74, ±14]	82	[80, ±17]	87	[86, ±19]
HIST	63	[63, ±9]	72	[72, ±11]	85	[83, ±15]	94	[92, ±17]	99	[96, ±19]	102	[100, ±20]	114	[111, ±24]	123	[119, ±27]
EOC4.5	63	[64, ±16]	74	[74, ±21]	87	[87, ±27]	96	[97, ±32]	102	[103, ±35]	106	[106, ±37]	119	[119, ±43]	128	[129, ±48]
EOC8.5	70	[70, ±16]	83	[83, ±21]	100	[100, ±27]	113	[112, ±32]	120	[119, ±34]	125	[124, ±36]	141	[140, ±43]	154	[152, ±47]
Grand Junction, CO																
PRISM	20	[20, ±2]	23	[23, ±3]	27	[27, ±5]	31	[29, ±6]	32	[31, ±7]	34	[32, ±7]	37	[35, ±9]	40	[38, ±10]
HIST	22	[22, ±2]	25	[24, ±3]	28	[27, ±4]	30	[30, ±5]	32	[31, ±5]	33	[32, ±6]	36	[35, ±6]	38	[37, ±7]
EOC4.5	27	[27, ±7]	32	[32, ±9]	39	[39, ±12]	44	[43, ±14]	46	[46, ±15]	48	[48, ±16]	55	[54, ±18]	59	[59, ±20]
EOC8.5	27	[27, ±6]	32	[32, ±8]	38	[37, ±10]	42	[42, ±12]	45	[44, ±13]	47	[46, ±14]	52	[52, ±17]	57	[56, ±19]
Minneapolis, MN																
PRISM	75	[77, ±17]	87	[89, ±22]	101	[104, ±29]	112	[115, ±34]	119	[122, ±37]	123	[126, ±38]	137	[141, ±45]	148	[152, ±50]
HIST	62	[63, ±12]	70	[71, ±15]	80	[81, ±20]	87	[88, ±23]	92	[92, ±25]	95	[95, ±26]	104	[105, ±31]	112	[112, ±35]
EOC4.5	82	[81, ±20]	97	[95, ±25]	117	[114, ±31]	131	[128, ±37]	140	[136, ±40]	146	[141, ±42]	165	[159, ±49]	179	[172, ±54]
EOC8.5	92	[91, ±16]	107	[105, ±20]	126	[122, ±27]	140	[135, ±31]	149	[143, ±33]	154	[148, ±35]	173	[165, ±41]	187	[178, ±45]
Nashville, TN																
PRISM	82	[81, ±10]	93	[91, ±12]	107	[104, ±16]	117	[114, ±19]	124	[119, ±20]	128	[123, ±22]	141	[136, ±25]	152	[146, ±28]
HIST	89	[91, ±17]	101	[103, ±22]	116	[118, ±29]	127	[130, ±34]	134	[137, ±38]	138	[142, ±40]	153	[157, ±47]	164	[168, ±52]
EOC4.5	106	[108, ±22]	124	[126, ±29]	146	[149, ±37]	162	[165, ±43]	172	[175, ±47]	178	[182, ±50]	200	[204, ±58]	216	[220, ±65]
EOC8.5	124	[122, ±25]	145	[142, ±30]	172	[168, ±38]	192	[187, ±44]	203	[198, ±47]	212	[206, ±49]	237	[231, ±58]	257	[251, ±64]
Phoenix, AZ																
PRISM	34	[34, ±8]	39	[39, ±10]	45	[45, ±13]	50	[50, ±15]	53	[52, ±17]	55	[54, ±17]	61	[61, ±20]	65	[65, ±23]
HIST	38	[37, ±6]	44	[43, ±7]	52	[51, ±9]	58	[57, ±11]	62	[61, ±12]	64	[63, ±13]	72	[71, ±15]	78	[76, ±16]
EOC4.5	43	[43, ±8]	51	[51, ±11]	62	[60, ±14]	69	[68, ±16]	74	[72, ±18]	77	[75, ±19]	87	[84, ±22]	95	[91, ±25]
EOC8.5	36	[36, ±8]	44	[44, ±11]	55	[54, ±13]	62	[61, ±16]	67	[65, ±17]	70	[68, ±18]	80	[78, ±20]	87	[85, ±23]
Seattle, WA																
PRISM	59	[61, ±14]	67	[70, ±19]	78	[81, ±25]	85	[89, ±29]	90	[94, ±31]	93	[97, ±33]	102	[108, ±39]	110	[116, ±43]
HIST	47	[47, ±4]	52	[51, ±5]	58	[57, ±6]	62	[61, ±7]	65	[63, ±8]	67	[65, ±8]	72	[70, ±9]	77	[74, ±11]
EOC4.5	44	[45, ±5]	48	[49, ±6]	53	[54, ±8]	56	[58, ±10]	58	[60, ±10]	60	[61, ±11]	65	[66, ±13]	68	[70, ±15]
EOC8.5	52	[54, ±11]	58	[60, ±14]	65	[69, ±19]	71	[75, ±22]	74	[78, ±24]	77	[81, ±25]	84	[89, ±30]	89	[95, ±33]
Tallahassee, FL																
PRISM	142	[146, ±38]	170	[175, ±49]	205	[212, ±62]	231	[239, ±72]	246	[254, ±78]	257	[265, ±82]	291	[301, ±96]	317	[326, ±106]
HIST	121	[126, ±34]	142	[148, ±44]	169	[177, ±58]	189	[198, ±68]	200	[211, ±75]	208	[219, ±79]	234	[246, ±91]	254	[266, ±100]
EOC4.5	159	[156, ±30]	189	[185, ±36]	228	[220, ±44]	256	[247, ±50]	273	[262, ±55]	284	[273, ±58]	322	[308, ±67]	350	[335, ±74]
EOC8.5	139	[136, ±32]	168	[163, ±39]	206	[199, ±49]	233	[225, ±55]	250	[240, ±59]	261	[251, ±62]	297	[285, ±72]	325	[311, ±79]

Fig. 9. Return periods (5–500 years) of daily precipitation (mm) for 1990–2005 (PRISM and HIST) and 2085–2100 (EOC4.5 and EOC8.5) for eight climatologically unique cities. The gradient represents the median of a 1000-iteration bootstrap for each city and the brackets contain the mean and 95% confidence interval.

Return periods can be complicated for communities and stakeholders to interpret, leading to inaccurate risk assessments and inadequate mitigation strategies. For example, a 100-year extreme daily precipitation event has a 1% chance of happening during any given year but a 39.4% chance of occurring within 50 years. While return periods can be challenging, the 100-year return period of daily precipitation values is often used in infrastructure design to reduce

Accepted for publication in *Journal of Applied Meteorology and Climatology*. DOI 10.1175/JAMC-D-23-0206.1.

impacts and is similarly used in determining insurance premiums for the National Flood Insurance Program (NFIP) (Min et al. 2011; Wright et al. 2021; FEMA 2023).

The percent change above HIST in the EOC scenarios for the 100-year return period of daily precipitation values varied for each city but was generally 20% or greater, with very large (> 50%) increases shown in Albany, Minneapolis, and Nashville (Fig. 8a, d, e). Looking at larger areas, regions of the Intermountain West, Midwest, Southeast, and Northeast all showed increases in the 100-year return period daily precipitation values above HIST in the EOC scenarios (Fig. 10b, c). A 50% or greater increase was displayed in EOC4.5 for 4.6% of 30 km grid boxes and 12.6% of the EOC8.5 30 km grid boxes. Regionally, the percent increases in the 100-year return period of daily precipitation values in the EOC scenarios were approximately 50–100% above the HIST epoch, with higher increases more widespread in the EOC8.5 scenario. Increases in the 100-year return period precipitation value had statistically significant increases in EOC8.5 for areas of the Intermountain West, Southwest, and Northeast while EOC4.5 displayed only sporadic areas of significant increases (Fig. 10d, e). National averages for percent change in 100-year return period precipitation values display an overall increasing trend with +8% in EOC4.5 and +19.4% in EOC8.5 (Fig. 10d, e). These return period precipitation value changes align with previous studies showing increases in return period precipitation values for most of the CONUS historically and in future simulations, albeit with some slight magnitude variations (DeGaeano 2009; Dominguez et al. 2012; Kunkel et al. 2013a). Increases in return period precipitation values have significant implications for infrastructure, especially considering structures currently under construction that assume historical values.

Accepted for publication in *Journal of Applied Meteorology and Climatology*. DOI 10.1175/JAMC-D-23-0206.1.

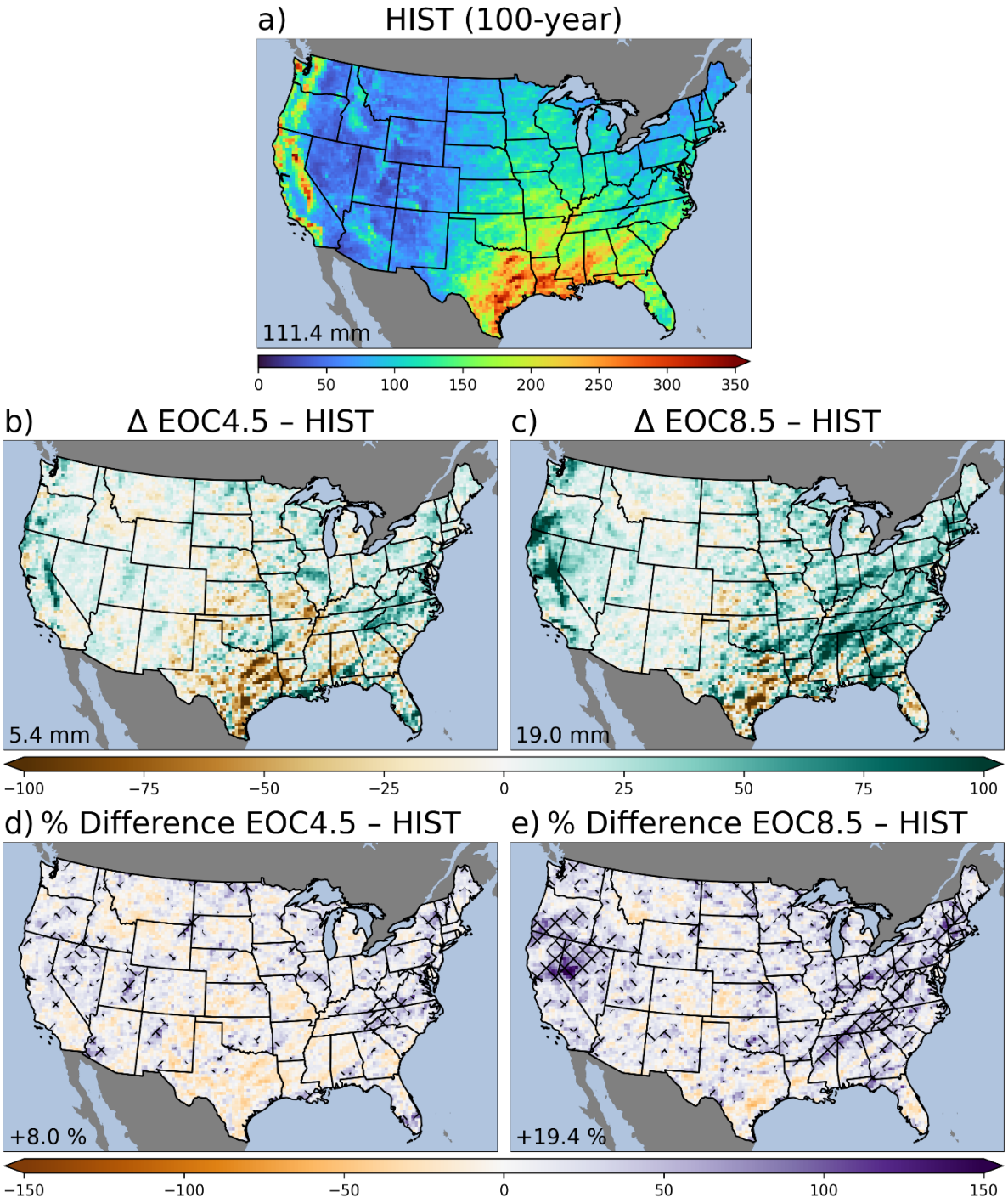

Fig. 10. 100-year return period daily precipitation values (mm) for 1990–2005 HIST (a), with raw (b, c) and percent (d, e) differences from HIST for 2085–2100 EOC4.5 and EOC8.5 epochs. Hatched areas on percent difference panels (third row) indicate regions where the median EOC epoch value was outside the HIST 95% confidence interval from a 1000-iteration bootstrap sample. National averages for each panel are displayed in the lower left.

4. Discussion and conclusions

Accepted for publication in *Journal of Applied Meteorology and Climatology*. DOI 10.1175/JAMC-D-23-0206.1.

We investigated how extreme daily precipitation—defined as the 99th percentile value in a 24-h period—may change by the end of the twenty-first century under two anthropogenic emissions scenarios using a novel convection-permitting dynamically downscaled RCM dataset with two end-of-century (2085–2100) epochs under pathways RCP4.5 and RCP8.5 (Table 3). The representation of smaller-scale features in RCMs permits explicit representations of hazardous convective weather, which is needed for resolving extreme daily precipitation. The simulated HIST epoch (1990–2005) of extreme daily precipitation compared favorably with some slight biases to an independent dataset of observations (PRISM) from the same time period, providing confidence in the analysis of future projections of extreme precipitation in the EOC scenarios (Table 3). Results projected increasing values of extreme daily precipitation through the end of the twenty-first century for both RCP scenarios in many regions in the CONUS, such as the Northeast, Midwest, Southeast, and Pacific Northwest (Table 3). For example, the 99th percentile daily precipitation value displayed increases greater than 20 mm in the Ohio Valley and Midwest (Dec–May). Several of these regions have historically seen increasing trends that could be exacerbated by anthropogenic climate change (e.g., Groisman et al. 2005; Alexander et al. 2006; Groisman et al. 2012; Kunkel et al. 2013a; Janssen et al. 2014; Huang et al. 2017; Changnon and Gensini 2019; Howarth et al. 2019). On the other hand, decreases in the 99th percentile of daily precipitation were found in the southern Great Plains in Dec–Feb. EVA further revealed an increasing ceiling for extremes in most of the eight climatologically unique cities examined, and daily precipitation return periods—a metric useful for insurance and engineering—showed robust increases above the 95% confidence interval of HIST by the end of the twenty-first century for one or both EOC scenarios in six of the eight cities examined.

	Dec–Feb	**Mar–May**	**Jun–Aug**	**Sept–Nov**
HIST Biases	Wet bias in the Intermountain West, northern Great Plains, and Midwest	Wet bias in the Intermountain West	Dry bias in the Intermountain West	Sporadic dry bias in the Southeast and wet bias in the Intermountain West
National Average	EOC4.5: 31.8 ±21.8 mm EOC8.5: 34.8 ±24.1 mm	EOC4.5: 31.5 ±15.6 mm EOC8.5: 32.3 ±17.6 mm	EOC4.5: 29.0 ±18.0 mm EOC8.5: 27.9 ±18.1 mm	EOC4.5: 29.6 ±15.0 mm EOC8.5: 30.4 ±16.2 mm
99th Percentile Changes	Sporadic increases across the Intermountain West in both EOC scenarios	Lower Midwest into the Ohio River Valley shows increases of 50–100% in EOC8.5	Robust decreases of 100–150% in the Intermountain West in EOC8.5	Sporadic areas of decrease in the Southwest, northern Great Plains, and Southeast in EOC8.5

Accepted for publication in *Journal of Applied Meteorology and Climatology*. DOI 10.1175/JAMC-D-23-0206.1.

Ohio and Tennessee River valleys and the Northeast display increases of 50–100% Decreases of 50–100% in the southern Great Plains in both EOC scenarios	Large decreases up to 100+% in the Southwest for EOC8.5	Sporadic decreases in the central and southern Great Plains in EOC8.5	Increases of ~100% in the central Midwest in EOC8.5

Table 3. 99th percentile of daily precipitation HIST biases, national average and standard deviation, and statistically significant changes across the CONUS.

Changes in the lower probability events (e.g., > 100-year return period) can have vast socioeconomic implications. The NFIP has Special Flood Hazard Areas (SFHA) which use a 100-year return period for floodplains, and those within a SFHA with a federally backed mortgage are required to have flood insurance (FEMA 2023). The NFIP floodplains differ slightly from the return periods calculated here since they use return periods based on the precipitation impact rather than amount. Both methods, however, communicate the risk associated with extreme precipitation events such that changes in return periods could change which locations are most vulnerable. Our results showed increases in precipitation values for return periods greater than 25 years in both EOC scenarios for all cities examined except Seattle, suggesting such changes in vulnerability are likely to occur. These socioeconomic implications highlight the importance of future work using land use and population projections for stakeholder awareness in adapting to and mitigating the effects of potential future changes in extreme precipitation.

Extreme hazards have low occurrence probabilities, yet the largest impacts, especially in current and projected regions of high risk and vulnerability due to increasing urbanization (e.g., Strader and Ashley 2015; Ferguson and Ashley 2017; Strader et al. 2017; Villarini and Slater 2017; Wing et al. 2018; Andreadis et al. 2022). Some communities in these regions lack the technological development and economic support to build resilience to these rare but impactful events, highlighting issues of interests, equity, and fairness in socioeconomically vulnerable areas and creating a window of opportunity to enact rapid policy change (Bubeck et al. 2017). Infrastructure is built with the intent of withstanding extreme events, yet precipitation extremes are projected to increase past the historical trends for many regions of the CONUS, threatening infrastructure survival against hazards in the future (Wright et al. 2021). Ultimately, this study illustrates that potential changes in extreme daily precipitation across various regions of the CONUS have the potential to impact numerous aspects of

Accepted for publication in *Journal of Applied Meteorology and Climatology*. DOI 10.1175/JAMC-D-23-0206.1.

society by the end of the twenty-first century. Using projected changes in precipitation risk in conjunction with other socioeconomic projections can aid stakeholders in planning for future disasters. Future work could focus on sub-daily accumulation for precipitation extremes. Additionally, taking a larger ensemble approach by using further emissions scenarios, GCM members, and time slices would help discern uncertainty of potential future changes in extreme precipitation.

Acknowledgments.

The authors would like to acknowledge high-performance computing support from Cheyenne (doi:10.5065/D6RX99HX) provided by NCAR's Computational and Information Systems Laboratory, sponsored by the National Science Foundation. This research was supported by the National Science Foundation awards 1637225 and 1800582. This research used resources of the Argonne Leadership Computing Facility, which is a DOE Office of Science User Facility supported under Contract DE-AC02-06CH11357.

Data Availability Statement.

All simulation output is available in netCDF format and stored on Argonne systems. The authors request that anyone interested in using the simulation output contact coauthor Gensini (vgensini@niu.edu) for information on how to access the data, including any collaboration.

REFERENCES

Adams, D. K., and A. C. Comrie, 1997: The North American Monsoon. *Bull. Amer. Meteor. Soc.*, **78**, 2197–2213, https://doi.org/10.1175/1520-0477(1997)078<2197:TNAM>2.0.CO;2.

Agel, L., M. Barlow, J.-H. Qian, F. Colby, E. Douglas, and T. Eichler, 2015: Climatology of Daily Precipitation and Extreme Precipitation Events in the Northeast United States. *J. Hydrometeor.*, **16**, 2537–2557, https://doi.org/10.1175/JHM-D-14-0147.1.

Alexander, L. V., and Coauthors, 2006: Global observed changes in daily climate extremes of temperature and precipitation. *J. Geophys. Res.*, **111**, D05109, https://doi.org/10.1029/2005JD006290.

Allan, R. P., and B. J. Soden, 2008: Atmospheric Warming and the Amplification of Precipitation Extremes. *Science*, **321**, 1481–1484, https://doi.org/10.1126/science.1160787.

Andreadis, K. M., O. E. J. Wing, E. Colven, C. J. Gleason, P. D. Bates, and C. M. Brown, 2022: Urbanizing the floodplain: global changes of imperviousness in flood-prone areas. *Environ. Res. Lett.*, **17**, 104024, https://doi.org/10.1088/1748-9326/ac9197.

Armal, S., N. Devineni, and R. Khanbilvardi, 2018: Trends in Extreme Rainfall Frequency in the Contiguous United States: Attribution to Climate Change and Climate Variability Modes. *J. Climate*, **31**, 369–385, https://doi.org/10.1175/JCLI-D-17-0106.1.

Ashley, S. T., and W. S. Ashley, 2008a: Flood Fatalities in the United States. *J. Appl. Meteor. Climatol.*, **47**, 805–818, https://doi.org/10.1175/2007JAMC1611.1.

Ashley, S. T., and W. S. Ashley, 2008b: The storm morphology of deadly flooding events in the United States. *Int. J. Climatol.*, **28**, 493–503, https://doi.org/10.1002/joc.1554.

Ashley, W. S., T. L. Mote, P. G. Dixon, S. L. Trotter, E. J. Powell, J. D. Durkee, and A. J. Grundstein, 2003: Distribution of Mesoscale Convective Complex Rainfall in the United States. *Mon. Wea. Rev.*, **131**, 3003–3017, https://doi.org/10.1175/1520-0493(2003)131<3003:DOMCCR>2.0.CO;2.

Ashley, W. S., S. Strader, T. Rosencrants, and A. J. Krmenec, 2014: Spatiotemporal Changes in Tornado Hazard Exposure: The Case of the Expanding Bull's-Eye Effect in Chicago, Illinois. *Wea. Climate Soc.*, **6**, 175–193, https://doi.org/10.1175/WCAS-D-13-00047.1.

Ashley, W. S., A. M. Haberlie, and V. A. Gensini, 2023: The Future of Supercells in the United States. *Bull. Amer. Meteor. Soc.*, **104**, E1–E21, https://doi.org/10.1175/BAMS-D-22-0027.1.

Asif, Z., Z. Chen, R. Sadiq, and Y. Zhu, 2023: Climate Change Impacts on Water Resources and Sustainable Water Management Strategies in North America. *Water Resour. Manage.*, **37**, 2771–2786, https://doi.org/10.1007/s11269-023-03474-4.

Bouwer, L. M., 2011: Have Disaster Losses Increased Due to Anthropogenic Climate Change? *Bull. Amer. Meteor. Soc.*, **92**, 39–46, https://doi.org/10.1175/2010BAMS3092.1.

Bruyère, C. L., J. M. Done, G. J. Holland, and S. Fredrick, 2014: Bias corrections of global models for regional climate simulations of high-impact weather. *Climate Dyn.*, **43**, 1847–1856, https://doi.org/10.1007/s00382-013-2011-6.

Bubeck, P., A. Otto, and J. Weichselgartner, 2017: Societal Impacts of Flood Hazards. *Oxford Research Encyclopedia of Natural Hazard Science*, Oxford University Press, https://doi.org/10.1093/acrefore/9780199389407.013.281.

Chan, S. C., E. J. Kendon, H. J. Fowler, S. Blenkinsop, N. M. Roberts, and C. A. T. Ferro, 2014: The Value of High-Resolution Met Office Regional Climate Models in the Simulation of Multihourly Precipitation Extremes. *J. Climate*, **27**, 6155–6174, https://doi.org/10.1175/JCLI-D-13-00723.1.

Changnon, D., and V. A. Gensini, 2019: Changing Spatiotemporal Patterns of 5- and 10-Day Illinois Heavy Precipitation Amounts, 1900–2018. *J. Appl. Meteor. Climatol.*, **58**, 1523–1533, https://doi.org/10.1175/JAMC-D-18-0335.1.

Creighton, G., E. Kuchera, R. Adams-Selin, J. McCormick, S. Rentschler, and B. Wickard, 2014: AFWA diagnostics in WRF. Air Force Weather Agency, 2nd Weather Group Doc., 17 pp., https://www2.mmm.ucar.edu/wrf/users/docs/AFWA_Diagnostics_in_WRF.pdf..

Coles, S., 2001: *An Introduction to Statistical Modeling of Extreme Values*. Springer, 228 pp.

Cook, B. I., J. S. Mankin, K. Marvel, A. P. Williams, J. E. Smerdon, and K. J. Anchukaitis, 2020: Twenty-first century drought projections in the CMIP6 forcing scenarios. *Earth's Future*, **8**, e2019EF001461, https://doi.org/10.1029/2019EF001461.

Dai, A., 2011: Drought under global warming: a review. *Wiley Interdiscip. Rev. Climate Change*, **2**, 45–65, https://doi.org/10.1002/wcc.81.

Dai, A., K. E. Trenberth, and T. Qian, 2004: A Global Dataset of Palmer Drought Severity Index for 1870–2002: Relationship with Soil Moisture and Effects of Surface Warming. *J. Hydrometeor.*, **5**, 1117–1130, https://doi.org/10.1175/JHM-386.1.

Daly, C., R. Neilson, and D. L. Phillips, 1994: A statistical-topographic model for mapping climatological precipitation. *J. Appl. Meteor.*, **33**, 140–158, https://doi.org/10.1175/1520-0450(1994)033<0140:ASTMFM>2.0.CO;2.

Daly, C., M. Halbleib, J. I. Smith, W. P. Gibson, M. K. Doggett, G. H. Taylor, J. Curtis, and P. P. Pasteris, 2008: Physiographically sensitive mapping of climatological temperature and precipitation across the conterminous United States. *Int. J. Climatol.*, **28**, 2031–2064, https://doi.org/10.1002/joc.1688.

Daly, C., and Coauthors, 2021: Challenges in observation-based mapping of daily precipitation across the conterminous United States. *J. Atmos. Oceanic Technol.*, **38**, 1979–1992, https://doi.org/10.1175/JTECH-D-21-0054.1.

Dee, D., and Coauthors, 2011: The ERA-Interim reanalysis: Configuration and performance of the data assimilation system. *Quart. J. Roy. Meteor. Soc.*, **137**, 553–597, https://doi.org/10.1002/qj.828.

DeGaetano, A. T., 2009: Time-Dependent Changes in Extreme-Precipitation Return-Period Amounts in the Continental United States. *J. Appl. Meteor. Climatol.*, **48**, 2086–2099, https://doi.org/10.1175/2009JAMC2179.1.

Dominguez, F., E. Rivera, D. P. Lettenmaier, and C. L. Castro, 2012: Changes in winter precipitation extremes for the western United States under a warmer climate as simulated by regional climate models. *Geophys. Res. Lett.*, **39**, L05803, https://doi.org/10.1029/2011GL050762.

FEMA, 2023: The National Flood Insurance Program (NFIP). Accessed 15 April 2023, www.fema.gov/national-flood-insurance-program.

Feng, Z., L. R. Leung, S. Hagos, R. A. Houze, C. D. Burleyson, and K. Balaguru, 2016: More frequent intense and long-lived storms dominate the springtime trend in central US rainfall. *Nat. Commun.*, **7**, 13429, https://doi.org/10.1038/ncomms13429.

Accepted for publication in *Journal of Applied Meteorology and Climatology*. DOI 10.1175/JAMC-D-23-0206.1.

Ferguson, A. P., and W. S. Ashley, 2017: Spatiotemporal analysis of residential flood exposure in the Atlanta, Georgia metropolitan area. *Nat. Hazards*, **87**, 989–1016, https://doi.org/10.1007/s11069-017-2806-6.

Fisher, R. A., and L. H. C. Tippett, 1928: Limiting forms of the frequency distribution of the largest or smallest member of a sample. *Math. Proc. Cambridge Philos. Soc.*, **24**, 180–190, https://doi.org/10.1017/S0305004100015681.

Fowler, H. J., and Coauthors, 2021: Anthropogenic intensification of short-duration rainfall extremes. *Nat. Rev. Earth Environ.,* **2**, 107–122, https://doi.org/10.1038/s43017-020-00128-6.

Friederichs, P., 2010: Statistical downscaling of extreme precipitation events using extreme value theory. *Extremes*, **13**, 109–132, https://doi.org/10.1007/s10687-010-0107-5.

Gensini, V. A., and T. L. Mote, 2014: Estimations of Hazardous Convective Weather in the United States Using Dynamical Downscaling. *J. Climate*, **27**, 6581–6589, https://doi.org/10.1175/JCLI-D-13-00777.1.

Gensini, V. A., A. M. Haberlie, and W. S. Ashley, 2023: Convection-permitting simulations of historical and possible future climate over the contiguous United States. *Climate Dyn.,* **60**, 109–126, https://doi.org/10.1007/s00382-022-06306-0.

Gnedenko, B., 1943: On the limiting distribution of a supercritical branching process in a random environment (in French). *Ann. Math.*, **44**, 423–453, https://doi.org/10.2307/1968974.

Groisman, P. Y., R. W. Knight, D. R. Easterling, T. R. Karl, G. C. Hegerl, and V. N. Razuvaev, 2005: Trends in Intense Precipitation in the Climate Record. *J. Climate,* **18**, 1326–1350, https://doi.org/10.1175/JCLI3339.1.

Groisman, P. Ya., R. W. Knight, and T. R. Karl, 2012: Changes in Intense Precipitation over the Central United States. *J. Hydrometeor.*, **13**, 47–66, https://doi.org/10.1175/JHM-D-11-039.1.

Gumbel, E. J., 1958: *Statistics of Extremes*. Columbia University Press, 375 pp.

Haberlie, A. M., and W. S. Ashley, 2019: A Radar-Based Climatology of Mesoscale Convective Systems in the United States. *J. Climate*, **32**, 1591–1606, https://doi.org/10.1175/JCLI-D-18-0559.1.

Haberlie, A. M., W. S. Ashley, C. M. Battisto, and V. A. Gensini, 2022: Thunderstorm Activity Under Intermediate and Extreme Climate Change Scenarios. *Geophys. Res. Lett.*, **49**, e2022GL098779, https://doi.org/10.1029/2022GL098779.

Haberlie, A. M., W. S. Ashley, V. A. Gensini, and A. C. Michaelis, 2023: The ratio of mesoscale convective system precipitation to total precipitation increases in future climate change scenarios. *npj Climate Atmos. Sci.*, **6**, 150, https://doi.org/10.1038/s41612-023-00481-5.

Han, Z., and H. O. Sharif, 2021: Analysis of Flood Fatalities in the United States, 1959–2019. *Water*, **13**, 1871, https://doi.org/10.3390/w13131871.

Hazeleger, W., B. J. J. M. Van Den Hurk, E. Min, G. J. Van Oldenborgh, A. C. Petersen, D. A. Stainforth, E. Vasileiadou, and L. A. Smith, 2015: Tales of future weather. *Nat. Climate Change*, **5**, 107–113, https://doi.org/10.1038/nclimate2450.

Hoogewind, K. A., M. E. Baldwin, and R. J. Trapp, 2017: The Impact of Climate Change on Hazardous Convective Weather in the United States: Insight from High-Resolution Dynamical Downscaling. *J. Climate*, **30**, 10081–10100, https://doi.org/10.1175/JCLI-D-16-0885.1.

Howarth, M. E., C. D. Thorncroft, and L. F. Bosart, 2019: Changes in Extreme Precipitation in the Northeast United States: 1979–2014. *J. Hydrometeor.*, **20**, 673–689, https://doi.org/10.1175/JHM-D-18-0155.1.

Huang, H., J. M. Winter, E. C. Osterberg, R. M. Horton, and B. Beckage, 2017: Total and Extreme Precipitation Changes over the Northeastern United States. *J. Hydrometeor.*, **18**, 1783–1798, https://doi.org/10.1175/JHM-D-16-0195.1.

Huang, X., and S. Stevenson, 2021: Connections Between Mean North Pacific Circulation and Western US Precipitation Extremes in a Warming Climate. *Earth's Future*, **9**, e2020EF001944, https://doi.org/10.1029/2020EF001944.

Hurrell, J. W., and Coauthors, 2013: The Community Earth System Model: A Framework for Collaborative Research. *Bull. Amer. Meteor. Soc.*, **94**, 1339–1360, https://doi.org/10.1175/BAMS-D-12-00121.1

IPCC, 2014: Climate Change 2014: Synthesis Report. R. K. Pachauri and L. A. Meyer, Eds., IPCC, 151 pp., www.ipcc.ch/report/ar5/syr/.

Janssen, E., D. J. Wuebbles, K. E. Kunkel, S. C. Olsen, and A. Goodman, 2014: Observational- and model-based trends and projections of extreme precipitation over the contiguous United States. *Earth's Future*, **2**, 99–113, https://doi.org/10.1002/2013EF000185.

Junker, N. W., R. S. Schneider, and S. L. Fauver, 1999: A study of heavy rainfall events during the great Midwest flood of 1993. *Wea. Forecasting*, **14**, 701–712, https://doi.org/10.1175/1520-0434(1999)014<0701:ASOHRE>2.0.CO;2.

Karl, T. R., and W. J. Koss, 1984: Regional and national monthly, seasonal, and annual temperature weighted by area, 1895-1983. National Climatic Data Center Historical Climatology Series 4-3, 38 pp.

Kharin, V. V., F. W. Zwiers, X. Zhang, and G. C. Hegerl, 2007: Changes in Temperature and Precipitation Extremes in the IPCC Ensemble of Global Coupled Model Simulations. *J. Climate*, **20**, 1419–1444, https://doi.org/10.1175/JCLI4066.1.

Kraft, L. L., G. Villarini, and J. Czajkowski, 2023: Characterizing the 2019 Midwest Flood: A Hydrologic and Socioeconomic Perspective. *Wea. Climate Soc.*, 15, 603–**617**, https://doi.org/10.1175/WCAS-D-22-0065.1.

Kumar, D., V. Mishra, and A. R. Ganguly, 2015: Evaluating wind extremes in CMIP5 climate models. *Climate Dyn.*, **45**, 441–453, https://doi.org/10.1007/s00382-014-2306-2.

Kunkel, K. E., D. R. Easterling, D. A. R. Kristovich, B. Gleason, L. Stoecker, and R. Smith, 2012: Meteorological Causes of the Secular Variations in Observed Extreme Precipitation Events for the Conterminous United States. *J. Hydrometeor.*, **13**, 1131–1141, https://doi.org/10.1175/JHM-D-11-0108.1.

Kunkel, K. E., and Coauthors, 2013a: Monitoring and Understanding Trends in Extreme Storms: State of Knowledge. *Bull. Amer. Meteor. Soc.*, **94**, 499–514, https://doi.org/10.1175/BAMS-D-11-00262.1.

Kunkel, K. E., T. R. Karl, D. R. Easterling, K. Redmond, J. Young, X. Yin, and P. Hennon, 2013b: Probable maximum precipitation and climate change. *Geophys. Res. Lett.*, **40**, 1402–1408, https://doi.org/10.1002/grl.50334.

Lackmann, G. M., 2013: The south-central U.S. flood of May 2010: Present and future. *J. Climate*, **26**, 4688–4709, https://doi.org/10.1175/JCLI-D-12-00392.1.

Lee, S., H. Nakagawa, K. Kawaike, and H. Zhang, 2016: Urban inundation simulation considering road network and building configurations. *J. Flood Risk Manag.*, **9**, 224–233, https://doi.org/10.1111/jfr3.12165.

Lenderink, G., and E. van Meijgaard, 2008: Increase in hourly precipitation extremes beyond expectations from temperature changes. *Nat. Geosci*, **1**, 511–514, https://doi.org/10.1038/ngeo262.

Li, Z., S. Gao, M. Chen, J. J. Gourley, and Y. Hong, 2022: Spatiotemporal Characteristics of US Floods: Current Status and Forecast Under a Future Warmer Climate. *Earth's Future*, **10**, https://doi.org/10.1029/2022EF002700.

Lim, J., and M. Skidmore, 2019: Flood Fatalities in the United States: The Roles of Socioeconomic Factors and the National Flood Insurance Program. *South. Econ. J.*, **85**, 1032–1057, https://doi.org/10.1002/soej.12330.

Loriaux, J. M., G. Lenderink, S. R. De Roode, and A. P. Siebesma, 2013: Understanding Convective Extreme Precipitation Scaling Using Observations and an Entraining Plume Model. *J. Atmos. Sci.*, **70**, 3641–3655, https://doi.org/10.1175/JAS-D-12-0317.1.

Makkonen, L., 2006: Plotting Positions in Extreme Value Analysis. *J. Appl. Meteor. Climatol.*, **45**, 334–340, https://doi.org/10.1175/JAM2349.1.

Meehl, G. A., J. M. Arblaster, and C. Tebaldi, 2005: Understanding future patterns of increased precipitation intensity in climate model simulations. *Geophys. Res. Lett.*, **32**, L18719, https://doi.org/10.1029/2005GL023680.

Accepted for publication in *Journal of Applied Meteorology and Climatology*. DOI 10.1175/JAMC-D-23-0206.1.

Min, S.-K., X. Zhang, F. W. Zwiers, and G. C. Hegerl, 2011: Human contribution to more-intense precipitation extremes. *Nature*, **470**, 378–381, https://doi.org/10.1038/nature09763.

Mishra, A. K., and V. P. Singh, 2010: A review of drought concepts. *J. Hydrol.*, **391**, 202–216, https://doi.org/10.1016/j.jhydrol.2010.07.012.

Moore, B. J., K. M. Mahoney, E. M. Sukovich, R. Cifelli, and T. M. Hamill, 2015: Climatology and Environmental Characteristics of Extreme Precipitation Events in the Southeastern United States. *Mon. Wea. Rev.*, **143**, 718–741, https://doi.org/10.1175/MWR-D-14-00065.1.

Moss, R. H., and Coauthors, 2010: The next generation of scenarios for climate change research and assessment. *Nature*, **463**, 747–756, https://doi.org/10.1038/nature08823.

National Academies of Sciences, Engineering, and Medicine, 2019: Framing the Challenge of Urban Flooding in the United States. *National Academies Press*, 100 pp., https://doi.org/10.17226/25381.

Naumann, G., and Coauthors, 2018: Global changes in drought conditions under different levels of warming. *Geophys. Res. Lett.*, **45**, 3285–3296, https://doi.org/10.1002/2017GL076521.

NCEI, 2023: U.S. Billion-Dollar Weather and Climate Disaster. NOAA/National Centers for Environmental Information, accessed February 2023, http://www.ncdc.noaa.gov/billions.

O'Gorman, P. A., 2012: Sensitivity of tropical precipitation extremes to climate change. *Nat. Geosci*, **5**, 697–700, https://doi.org/10.1038/ngeo1568.

O'Gorman, P. A., and T. Schneider, 2009: Scaling of Precipitation Extremes over a Wide Range of Climates Simulated with an Idealized GCM. *J. Climate*, **22**, 5676–5685, https://doi.org/10.1175/2009JCLI2701.1.

Pan, L.-L., S.-H. Chen, D. Cayan, M.-Y. Lin, Q. Hart, M.-H. Zhang, Y. Liu, and J. Wang, 2011: Influences of climate change on California and Nevada regions revealed by a high-resolution dynamical downscaling study. *Climate Dyn.*, **37**, 2005–2020, https://doi.org/10.1007/s00382-010-0961-5.

Accepted for publication in *Journal of Applied Meteorology and Climatology*. DOI 10.1175/JAMC-D-23-0206.1.

Papalexiou, S. M., and A. Montanari, 2019: Global and regional increase of precipitation extremes under global warming. *Water Resour. Res.*, **55**, 4901–4914, https://doi.org/10.1029/2018WR024067.

Perica, S., S. Pavlovic, M. St. Laurent, C. Trypaluk, D. Unruh, D. Martin, and O. Wilhite, 2015 (revised 2019): *Precipitation-Frequency Atlas of the United States.* Vol. 10, *NOAA Atlas 14*, NOAA, National Weather Service, 265 pp., https://www.weather.gov/media/owp/oh/hdsc/docs/Atlas14_Volume10.pdf.

Perica, S., and Coauthors, 2013: *Southeastern States (Alabama, Arkansas, Florida, Georgia, Louisiana, Mississippi)*. Vol. 9, version 2, *Precipitation-Frequency Atlas of the United States*, NOAA Atlas 14, 163 pp., https://www.weather.gov/media/owp/hdsc_documents/Atlas14_Volume9.pdf.

Picard, C. J., J. M. Winter, C. Cockburn, J. Hanrahan, N. G. Teale, P. J. Clemins, and B. Beckage, 2023: Twenty-first century increases in total and extreme precipitation across the Northeastern USA. *Climatic Change*, **176**, 72, https://doi.org/10.1007/s10584-023-03545-w.

Powers, J. G., and Coauthors, 2017: The Weather Research and Forecasting Model: Overview, System Efforts, and Future Directions. *Bull. Amer. Meteor. Soc.*, **98**, 1717–1737, https://doi.org/10.1175/BAMS-D-15-00308.1.

Prein, A. F., and Coauthors, 2015: A review on regional convection-permitting climate modeling: Demonstrations, prospects, and challenges. *Rev. Geophys.*, **53**, 323–361, https://doi.org/10.1002/2014RG000475.

Prein, A. F., C. Liu, K. Ikeda, S. B. Trier, R. M. Rasmussen, G. J. Holland, and M. P. Clark, 2017: Increased rainfall volume from future convective storms in the US. *Nat. Climate Change*, **7**, 880–884, https://doi.org/10.1038/s41558-017-0007-7.

Quintero, F., G. Villarini, A. F. Prein, W. F. Krajewski, and W. Zhang, 2022: On the role of atmospheric simulations horizontal grid spacing for flood modeling. *Climate Dyn.*, **59**, 3167–3174, https://doi.org/10.1007/s00382-022-06233-0.

Rashid, M. M., T. Wahl, G. Villarini, and A. Sharma, 2023: Fluvial Flood Losses in the Contiguous United States Under Climate Change. *Earth's Future*, **11**, https://doi.org/10.1029/2022EF003328.

Robinson, E. D., R. J. Trapp, and M. E. Baldwin, 2013: The geospatial and temporal distributions of severe thunderstorms from high-resolution dynamical downscaling. *J. Appl. Meteor. Climatol.*, **52**, 2147–2161, https://doi.org/10.1175/JAMC-D-12-0131.1.

Schär, C., and Coauthors, 2016: *Climatic Change*, **137**, 201–216, https://doi.org/10.1007/s10584-016-1669-2.

Schumacher, R. S., and R. H. Johnson, 2006: Characteristics of U.S. Extreme Rain Events during 1999–2003. *Wea. Forecasting*, **21**, 69–85, https://doi.org/10.1175/WAF900.1.

Shepherd, T. G., and Coauthors, 2018: Storylines: an alternative approach to representing uncertainty in physical aspects of climate change. *Climatic Change*, **151**, 555–571, https://doi.org/10.1007/s10584-018-2317-9.

Sillmann, J., and E. Roeckner, 2008: Indices for extreme events in projections of anthropogenic climate change. *Climatic Change*, **86**, 83–104, https://doi.org/10.1007/s10584-007-9308-6.

Skamarock, W. C., and J. B. Klemp, 2008: A time-split nonhydrostatic atmospheric model for weather research and forecasting applications. *J. Comput. Phys.*, **227**, 3465–3485, https://doi.org/10.1016/j.jcp.2007.01.037.

Skamarock, W. C., and Coauthors, 2019: A description of the Advanced Research WRF Model version 4. NCAR Tech. Note NCAR/TN-556+STR, 145 pp., https://doi.org/10.5065/1dfh-6p97.

Stevenson, S. N., and R. S. Schumacher, 2014: A 10-Year Survey of Extreme Rainfall Events in the Central and Eastern United States Using Gridded Multisensor Precipitation Analyses. *Mon. Wea. Rev.*, **142**, 3147–3162, https://doi.org/10.1175/MWR-D-13-00345.1.

Strader, S. M., and W. S. Ashley, 2015: The Expanding Bull's-Eye Effect. *Weatherwise*, **68**, 23–29, https://doi.org/10.1080/00431672.2015.1067108.

Accepted for publication in *Journal of Applied Meteorology and Climatology*. DOI 10.1175/JAMC-D-23-0206.1.

Strader, S. M., W. S. Ashley, T. J. Pingel, and A. J. Krmenec, 2017: Projected 21st century changes in tornado exposure, risk, and disaster potential. *Climatic Change*, **141**, 301–313, https://doi.org/10.1007/s10584-017-1905-4.

Stinnett, S. N., 2023: Historical and Potential Future Climate of Extreme Daily Precipitation over the Contiguous United States Using Convection-Permitting Simulations. M.S. thesis, Dept. of Earth, Atmosphere, and Environment, Northern Illinois University. 84 pp.

Sugiyama, M., H. Shiogama, and S. Emori, 2010: Precipitation extreme changes exceeding moisture content increases in MIROC and IPCC climate models. *Proc. Natl. Acad. Sci. USA*, **107**, 571–575, https://doi.org/10.1073/pnas.0903186107.

Tabari, H., 2021: Extreme value analysis dilemma for climate change impact assessment on global flood and extreme precipitation. *J. Hydrol.*, **593**, 125932, https://doi.org/10.1016/j.jhydrol.2020.125932.

Taylor, K. E., R. J. Stouffer, and G. A. Meehl, 2012: An Overview of CMIP5 and the Experiment Design. *Bull. Amer. Meteor. Soc.*, **93**, 485–498, https://doi.org/10.1175/BAMS-D-11-00094.1.

Tippett, M. K., J. T. Allen, V. A. Gensini, and H. E. Brooks, 2015: Climate and Hazardous Convective Weather. *Curr. Climate Change Rep.*, **1**, 60–73, https://doi.org/10.1007/s40641-015-0006-6.

Trapp, R. J., E. D. Robinson, M. E. Baldwin, N. S. Diffenbaugh, and B. R. J. Schwedler, 2011: Regional climate of hazardous convective weather through high-resolution dynamical downscaling. *Climate Dyn.*, **37**, 677–688, https://doi.org/10.1007/s00382-010-0826-y.

Trapp, R. J., K. A. Hoogewind, and S. Lasher-Trapp, 2019: Future changes in hail occurrence in the United States determined through convection-permitting dynamical downscaling. *J. Climate*, **32**, 5493–5509, https://doi.org/10.1175/JCLI-D-18-0740.1.

Trenberth, K. E., 2011: Changes in precipitation with climate change. *Climate Res.*, **47**, 123–138, https://doi.org/10.3354/cr00953.

Trenberth, K. E., A. Dai, R. M. Rasmussen, and D. B. Parsons, 2003: The Changing Character of Precipitation. *Bull. Amer. Meteor. Soc.*, **84**, 1205–1218, https://doi.org/10.1175/BAMS-84-9-1205.

Trenberth, K. E., A. Dai, G. van der Schrier, P. D. Jones, J. Barichivich, K. R. Briffa, and J. Sheffield, 2014: Global warming and changes in drought. *Nat. Climate Change*, **4**, 17–22, https://doi.org/10.1038/nclimate2067.

Ukkola, A. M., M. G. D. Kauwe, M. L. Roderick, G. Abramowitz, and A. J. Pitman, 2020: Robust future changes in meteorological drought in CMIP 6 projections despite uncertainty in precipitation. *Geophys. Res. Lett.*, **47**, e2020GL087820, https://doi.org/10.1029/2020GL087820.

Villarini, G., and L. Slater, 2017: Climatology of flooding in the United States. *Oxford Research Encyclopedia of Natural Hazard Science,* S. L. Cutter, Ed., Oxford University Press, https://doi.org/10.1093/acrefore/9780199389407.013.123.

Weisman, M. L., W. C. Skamarock, and J. B. Klemp, 1997: The resolution dependence of explicitly modeled convective systems. *Mon. Wea. Rev.*, **125**, 527–548, https://doi.org/10.1175/1520-0493(1997)125<0527:TRDOEM>2.0.CO;2.

Westra, S., L. V. Alexander, and F. W. Zwiers, 2013: Global Increasing Trends in Annual Maximum Daily Precipitation. *J. Climate*, **26**, 3904–3918, https://doi.org/10.1175/JCLI-D-12-00502.1.

Westra, S., and Coauthors, 2014: Future changes to the intensity and frequency of short-duration extreme rainfall. *Rev. Geophys.*, **52**, 522–555, https://doi.org/10.1002/2014RG000464.

Wing, O. E. J., P. D. Bates, A. M. Smith, C. C. Sampson, K. A. Johnson, J. Fargione, and P. Morefield, 2018: Estimates of present and future flood risk in the conterminous United States. *Environ. Res. Lett.*, **13**, 034023, https://doi.org/10.1088/1748-9326/aaac65.

Wright, D. B., C. Samaras, and T. Lopez-Cantu, 2021: Resilience to Extreme Rainfall Starts with Science. *Bull. Amer. Meteor. Soc.***102**, E808–E813, https://doi.org/10.1175/BAMS-D-20-0267.1.

Wuebbles, D. J., D. W. Fahey, K. A. Hibbard, D. J. Dokken, B. C. Stewart, and T. K. Maycock, Eds., 2017: *Climate Science Special Report: Fourth National Climate Assessment.* Vol. I, U.S. Global Change Research Program, 470 pp., https://doi.org/10.7930/J0J964J6.

Zhang, W., and G. Villarini, 2017: On the unseasonal flooding over the Central United States during December 2015 and January 2016. *Atmos. Res.*, **196**, 23–28, https://doi.org/10.1016/j.atmosres.2017.05.014.

Zhang, F., J. A. Biederman, M. P. Dannenberg, D. Yan, S. C. Reed, and W. K. Smith, 2021: Five decades of observed daily precipitation reveal longer and more variable drought events across much of the western United States. *Geophys. Res. Lett.*, **48**, e2020GL092293, https://doi.org/10.1029/2020GL092293.

Zhou, Q., G. Leng, and J. Peng, 2018: Recent Changes in the Occurrences and Damages of Floods and Droughts in the United States. *Water*, **10**, 1109, https://doi.org/10.3390/w10091109.

Zhou, Q., G. Leng, J. Su, and Y. Ren, 2019: Comparison of urbanization and climate change impacts on urban flood volumes: Importance of urban planning and drainage adaptation. *Sci. Total Environ.*, **658**, 24–33, https://doi.org/10.1016/j.scitotenv.2018.12.184.

Zhu, J., W. Forsee, R. Schumer, and M. Gautam, 2013: Future projections and uncertainty assessment of extreme rainfall intensity in the United States from an ensemble of climate models. *Climatic Change*, **118**, 469–485, https://doi.org/10.1007/s10584-012-0639-6.